Aus der Klinik für Innere Medizin,
Schwerpunkt Gastroenterologie, Endokrinologie, Stoffwechsel
und klinische Infektiologie
Geschäftsführender Direktor: Prof. Dr. Thomas M. Gress

des Fachbereichs Medizin der Philipps-Universität Marburg

Synthetic lethal interactions between *ATR* and DNA polymerases as a novel concept for individualized cancer therapy

Inaugural-Dissertation
zur Erlangung des Doktorgrades der Naturwissenschaften
(Dr. rer. nat.)
dem Fachbereich Medizin der Philipps-Universität Marburg
vorgelegt von

Albert Job
aus Kurgan-Tjube, Tadschikistan

Marburg, 2019

Angenommen vom Fachbereich Medizin der Philipps-Universität Marburg am: 12.08.2019

Gedruckt mit Genehmigung des Fachbereichs Medizin.

Dekan:	Prof. Dr. Helmut Schäfer
Referent:	Prof. Dr. Eike Gallmeier
1. Korreferent:	Prof. Dr. Thorsten Stiewe
2. Korreferent:	Prof. Dr. Guntram Suske

Contents

Indices

Abbreviations

5-FU	5-fluorouracil
ATR	ataxia telangiectasia and Rad3-related protein
BRCA1/2	breast cancer 1 or 2
BSA	bovine serum albumin
cDNA	complementary DNA
CldU	5-chloro-2′-deoxyuridine
COSMIC	Catalogue Of Somatic Mutations In Cancer
CRC	colorectal cancer
ctrl	control
DAPI	4',6-diamidino-2-phenylindole
ddNTP	dideoxyribonucleotide triphosphate
DDR	DNA damage response
DMSO	dimethyl sulfoxide
dNTP	deoxyribonucleotide triphosphate
DSB	double-strand break
DTT	dithiothreitol
FBS	fetal bovine serum
gRNA	guide RNA
HR	homologous recombination
HRP	horseradish peroxidase
HU	hydroxyurea
ICL	interstrand-crosslinking
IdU	5-iodo-2′-deoxyuridine
IR	ionizing radiation
KO	knockout
LHA	left homology arm
MCM	minichromosome maintenance
MMC	mitomycin C
NTC	nontransfected cells
PAM	protospacer adjacent motif
PARP	poly (ADP-ribose) polymerase

PBS	phosphate buffered saline
PMSF	phenylmethylsulfonyl fluoride
Pol	polymerase
pre-RC	pre-replication complex
PuroR	puromycin resistance
PVDF	polyvinylidene fluoride
RHA	right homology arm
RT	room temperature
SDS	sodium dodecyl sulfate
siPRIM1	siRNA targeting *PRIM1*
siRNA	small interfering RNA
ssDNA	single-strand DNA
TLS	translesion DNA synthesis
VUS	variant of uncertain significance
WT	wild type

Figures

Tables

1 Introduction

1.1 Cancer

Malignant tumors, colloquially often termed cancer, arise from autologous cells through the accumulation of various genetic alterations, which frequently occur in proto-oncogenes and/or tumor suppressor genes. This process is called malignant transformation. Proto-oncogenes, which encode for growth factor receptors or transcription factors, regulate cell proliferation. Genetic alterations affecting protein function, gene expression, or copy number result in uncontrolled cell proliferation. Proto-oncogenes altered by such a gain-of-function variant are called oncogenes. The fusion gene *BCR-ABL1*, a hyper-active tyrosine kinase caused by chromosomal translocation, induces chronic myeloid leukemia, and is one example for oncogenes giving rise to cancer [24]. Tumor suppressor genes and their subgroup of genome maintenance genes regulate the cellular processes of cell cycle progression or apoptosis as well as DNA repair, respectively. Genetic alterations within these genes result in a loss-of-function and thus in accumulation of DNA damage and/or a disturbed balance between cell proliferation and apoptosis. One prominent example for a genetically altered tumor suppressor gene in various cancers is *TP53*, which encodes the well studied transcription factor p53 protein [64]. Additionally to proto-oncogenes and tumor suppressor genes, genetic alterations are also necessary in genes responsible for cell metabolism or angiogenesis to overcome the tumor's increased need for nutrients, energy, and oxygen [65, 96]. Such genetic alterations often occur spontaneously, but may also be caused by exogenous factors, including ionizing radiation, pathogens (e. g. human papillomavirus), or chemicals, like benzene.

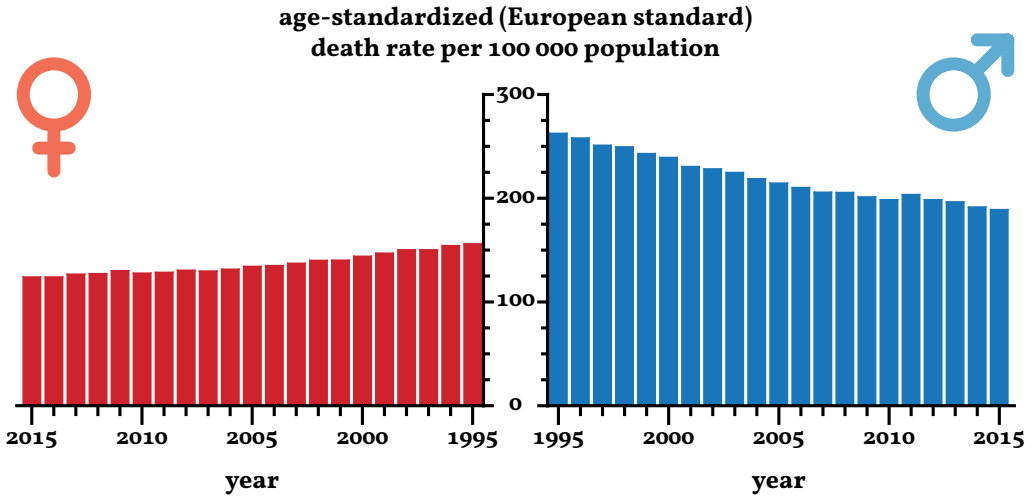

Figure 1 | Cancer caused death rate in Germany
Depiction of the age-standardized (European standard) death rate caused by cancer per 100 000 population for female (left) and male (right) in Germany, which is continuously decreasing in the last two decades from 1995 to 2015 [35].

In 2015 cancer was the cause of about 25 % of all deaths (925 200) in Germany, and although it represents the second most common cause of death after diseases of the cardiovascular system [90] the death rate in the last two decades in Germany is continuously decreasing (Figure 1) [35]. On the one hand, this may be explained by diagnostic procedures, getting more sensitive, and a broader range of preventive checkups, enabling an early cancer diagnosis and treatment, thus increasing survival rates. On the other hand, research led to various additional and more specific therapeutic approaches. So far, there are three approaches for cancer therapy, which are the surgical resection of the tumor, the radio- as well as the chemotherapy. The disadvantages of these approaches are the inoperability of some tumors due to their localization and the toxicity of the radio- and chemotherapy not only for cancer cells but also for healthy cells. The latter two causing severe negative side effects, including diarrhea, vomiting, hair loss, or bone marrow suppression. Consequentially, this resulted in the necessity of therapies being individualized and targeted, and finally led to a fourth approach in cancer therapy: the targeted therapy. A successful and already clinically applicable approach of targeted therapy is based on small molecules or monoclonal antibodies, impairing the target's protein function to aim at tumors with oncogenic gain-of-function variants [52]. One such example is the treatment of chronic myeloid leukemia patients with imatinib (brand name Glivec), targeting the already mentioned hyper-active fusion tyrosine kinase *BCR-ABL1* [15]. The treatment of tumors with defects in tumor suppressor/genome maintenance genes with inhibiting small molecules is not possible, as the protein function is already impaired due to their loss-of-function variants. However, the defective tumor suppressor/genome maintenance genes cause an increased sensitivity to agents inducing additional DNA damage, like interstrand-crosslinking (ICL)

agents, thus representing one approach to treat tumors with loss-of-function variants. Furthermore, tumors with defective tumor suppressor/genome maintenance genes are hyper-dependent on other compensatory DNA repair pathways. These relationships could be attributable to synthetic lethal interactions, and thus offer another therapeutic approach to treat tumors with loss-of-function variants. The concept of synthetic lethality and its clinical significance are described below.

1.2 Synthetic lethality

Synthetic lethality describes a relationship between two genes, in which the impairment of one of these two genes is not lethal, but the combined impairment of both genes results in cell death. The concept was first described by Calvin Bridges in 1922, who observed lethality in a *Drosophila melanogaster* population due to the combination of certain alterations [10]. Later the term "synthetic lethality" was coined by Theodore Dobzhansky in 1946 [22]. Although, this concept was originally described as an alteration-mediated gene impairment, it is today also applied to protein impairment mediated by chemical compounds. From a clinical perspective, synthetic lethality offers a novel concept of therapy for cancer patients. As cancers often accumulate characteristic gene defects during the process of tumorigenesis (Figure 2a + b), they become hyper-dependent on genes, which have a synthetic lethal relationship to the defective cancer driven gene, and thus compensate its functional loss. Applying a chemical inhibitor targeting this compensatory gene would induce synthetic lethality, and ultimately result in cell death (Figure 2c). Thus, patients would benefit from a tumor-genotype specific cancer therapy with less negative side effects, as the inhibitor treatment would only target cancer but not healthy cells [46].

The potential applicability of synthetic lethality for an individualized and targeted cancer treatment was already suggested in 1997 by Hartwell *et al.* [39], before 2005 two groups showed the possibility to treat cancers with deficiencies in the breast cancer 1 or 2 (*BRCA1/2*) genes, both involved in the repair of DNA double-strand breaks (DSBs) via homologous recombination (HR), with inhibitors targeting poly (ADP-ribose) polymerase (PARP), a protein involved in DNA repair, by exploiting their synthetic lethal relationship [11, 27]. These data led to the investigation of various PARP inhibitors in clinical trials (comprehensively reviewed by Lord & Ashworth [55]), and ultimately in 2014 to the first clinical approval of drugs exploiting synthetic lethality by the U. S. Food and Drug Administration and the European Medicines Agency. Beside *BRCA1/2* and *PARP*, as the probably most prominent example for clinical applicability of synthetic lethality, various other therapeutic approaches based on synthetic lethal relationships are currently investigated. One such example is the application of chemical inhibitors targeting

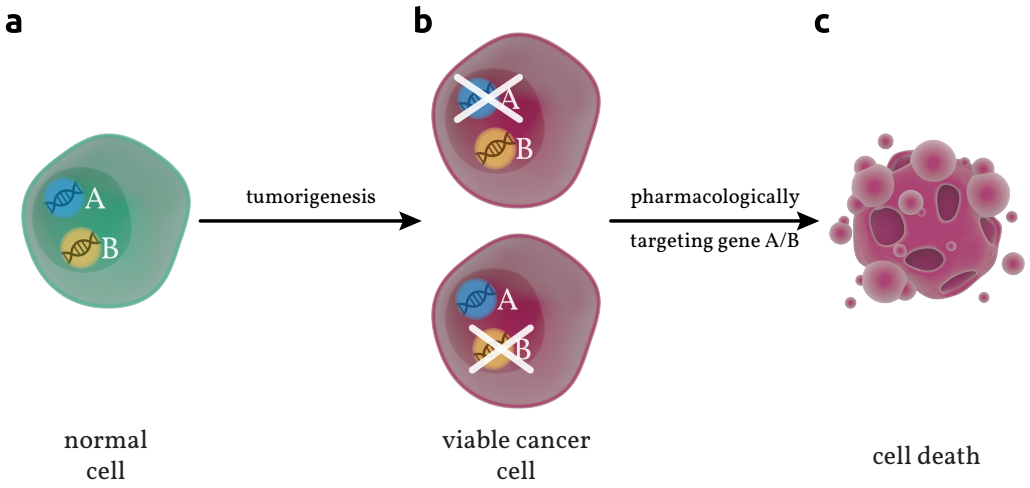

Figure 2 | The concept of synthetic lethality
a | A healthy cell with intact genes A and B. **b** | During the process of tumorigenesis, one of the two genes A or B becomes impaired due to genetic alterations. As the respective second gene compensates for the loss of the first genes, these cancers cells become hyper-dependent on the compensatory gene, but remain viable. **c** | Targeting the intact, compensatory gene with chemical inhibitors induces synthetic lethality and leads to cell death.

the ataxia telangiectasia and Rad3-related protein (ATR), a member of the DNA repair machinery, in tumors with defective *TP53* [80, 86, 88] or *KRAS* genes [36]. As potential synthetic lethal relationships are documented to be likely between DNA repair genes and DNA replication genes [29, 39], *ATR* and DNA polymerases could additionally represent promising synthetic lethal relationships. However, these relationships remained so far insufficiently identified or characterized, and thus should be further investigated.

1.3 Polymerases and the replication of DNA

The DNA polymerase (Pol) is an enzyme catalyzing the synthesis of DNA molecules from deoxyribonucleotides. Currently, at least 15 different polymerases are known in eukaryotes [44], which can be divided into translesion DNA synthesis (TLS) and replicative polymerases. TLS polymerases allow cells to complete replication despite damaged DNA templates by promoting the replication complex through DNA lesions, thus avoiding the halt of the replication process [93]. Along with their capability of DNA repair, TLS polymerases are marked by features like lack of 3'–5' exonuclease activity, low replication fidelity, the ability to copy a damaged DNA strand, or catalyzing the polymerization using aberrant primer DNA ends [8]. Replicative polymerases are responsible for the important process of replication of both mitochondrial DNA (Polγ) and genomic DNA. The latter process is performed by three major polymerases: the Polα-primase complex, Polδ, and Polε.

The error-free replication of genomic DNA is a fundamental and essential biological process of all living cells. Initiated during late M- to early G_1-phase, the origin recognition complex, consisting of six subunits of DNA binding proteins, binds to origins of replications within the genome. Subsequently, it recruits other proteins, including two copies of the hexameric minichromosome maintenance (MCM) complex with a 3'→5' polarity, and a yet dormant helicase activity to assemble the pre-replication complex (pre-RC). In this state, the origins of replications are "licensed" for activation. Upon entry into S-phase, other essential replication proteins, including the tetrameric GINS complex and Cdc45, are loaded onto the pre-RC, and together with the separation of the double MCM complex into two single MCM complexes activate the helicase activity. The two DNA helicases unwind the DNA according to their 3'→5' polarity in opposite directions, thus forming a replication bubble, and the resulting single-strand DNA (ssDNA) is stabilized and protected from degradation by being coated with RPA (Figure 3) [5, 12, 57].

The subsequent elongation step of the DNA replication is initiated by the Polα-primase complex. This heterotetrameric protein consists of the two catalytic subunits *PRIM1* and *POLA1*, which confer primase and polymerase activities, respectively, and the two regulatory subunits *PRIM2* and *POLA2*. Primase has the unique ability to synthesize RNA primer with an average length of 7–9 nucleotides *de novo*, which are then furtherly elongated by Polα to form RNA-DNA hybrid primer with a

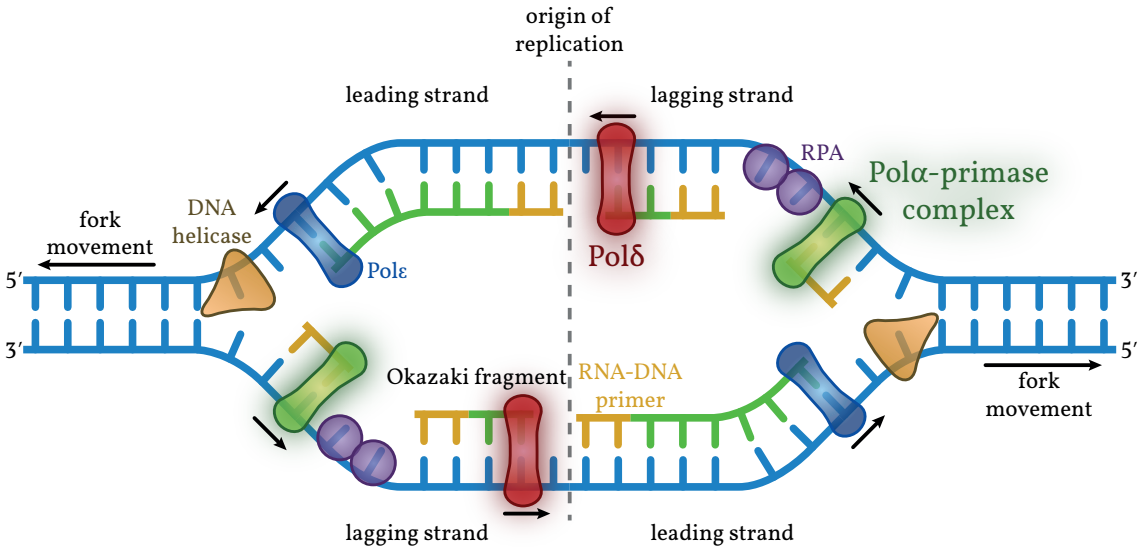

Figure 3 | Schematic illustration of a replication bubble
Starting at origins of replication, two DNA helicases unwind DNA in opposite directions mediated by their 3'–5' polarity, and thus creating a replication bubble. The ssDNA is coated by RPA to stabilize and protect it from degradation, while the Polα-primase complex synthesizes RNA-DNA hybrid primer. These serve as starting point for the continuous elongation of the leading strand by Polε and the discontinuous elongation of the lagging strand by Polδ, resulting in Okazaki fragments. The polymerases α-primase and δ were further investigated in this dissertation and thus highlighted. Figure modified from Russell [85].

length of 20–40 nucleotides [49, 77, 97], serving as starting point for the elongation of the two separated DNA strands by the polymerases δ and ε. The similarity of the moving direction between these two polymerases and the DNA helicase, i. e. 3'→5' along the parental DNA strand, results in differences of elongation of the two separated DNA strands. The synthesis of the new 5'–3' DNA strand is continuously, as the polymerase moves in the same direction as the DNA helicase. This DNA strand is thus referred to as leading strand, and mainly, but not exclusively elongated by Polε, whose catalytic subunit is encoded by *POLE* [40]. The synthesis of the new 3'–5' DNA strand, however, is discontinuous, as the polymerase is forced to move in the opposite direction of the DNA helicase, and thus can only synthesize short DNA strands, the so called Okazaki fragments. Hence, this DNA strand is referred to as lagging strand, and mainly, but not exclusively elongated by Polδ. It consists of the catalytic subunit *POLD1* and the three regulatory subunits *POLD2*, *POLD3*, and *POLD4*. Beside its polymerase activity, Polδ also has 3'–5' exonuclease proofreading activity, and is thus additionally involved in DNA repair synthesis [23, 67, 72].

As polymerases, especially the replicative DNA polymerases Polα-primase complex, Polδ, and Polε, are responsible for both the fundamental processes of DNA replication as well as DNA repair, it is obvious that a proper functionality of these proteins is crucial for the continuity of a cell's viability. Therefore, any defects in genes encoding for polymerases could result in accumulated genetic alterations and a hence increased risk of tumorigenesis. In fact, defects in the TLS polymerase η (encoded by the *POLH* gene), for example, result in a certain type of the xeroderma pigmentosum disease with increased susceptibility to skin cancer [59]. Additionally, multiple variants of uncertain significance (VUS)—these are genetically altered alleles with unknown impact on the protein's function or a potential pathogenic outcome [82]—within the polymerases δ and ε have been identified in various cancers [7, 74, 94]. As mentioned earlier, tumors with defective tumor suppressor/genome maintenance genes, including polymerases, might be treated by exploiting their synthetic lethal interactions. However, the question which genes might act synthetically lethal with certain polymerases has yet been insufficiently answered, and thus was investigated in this dissertation.

1.4 ATR and the DNA damage response

The genome is continually exposed to high levels of DNA damage. Various molecular mechanisms evolved to maintain genome integrity, and the entirety of these mechanisms is known as DNA damage response (DDR). Key regulators of DDR are ATM and ATR, both members of the phosphoinositide 3-kinase-related kinase family. ATM regulates—either directly or through its main effector kinase CHK2—various

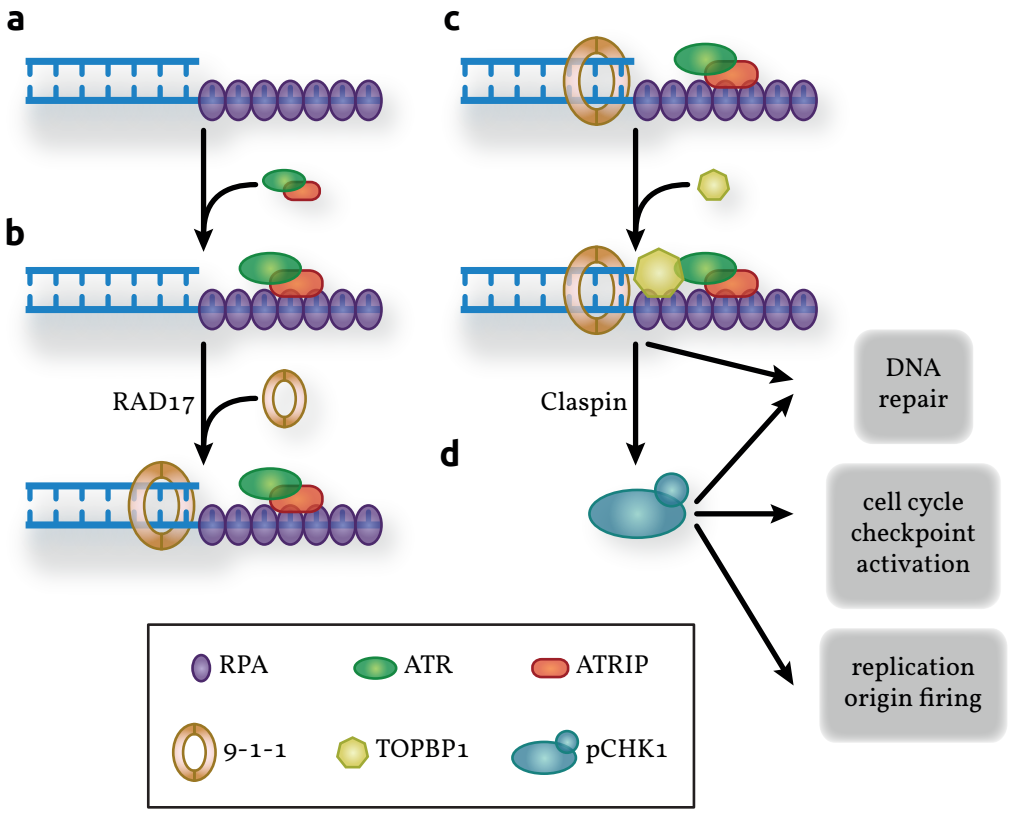

Figure 4 | Recruitment and activation of ATR
a | RPA coats ssDNA, which accumulates during stalled replication forks or certain DNA repair mechanisms, to stabilize and protect it from premature degradation. **b** | The ability of ATRIP, which is associated with ATR, to directly interact with ssDNA-bound RPA localizes ATR to sites of stalled replication forks or DNA damage. Additionally, RPA interacts with RAD17, and thereby recruits the 9-1-1 complex. **c** | This complex then recruits TOPBP1, which is thought to be the critical step in ATR activation. Activated ATR further participates in DNA repair mechanism and, **d** | mediated by Claspin, also phosphorylates and thereby activates CHK1, which is responsible for the induction of mechanisms involved in DNA repair, cell cycle checkpoint activation, and replication origin firing. Figure modified from Rundle *et al.* [84].

signal transduction pathways including DNA repair, cell cycle arrest, or gene expression, and is activated by the formation of DSB. The structural elements that result in ATR activation are ssDNA. These accumulate during stalled replication forks or the nucleoside excision repair mechanism, and are coated by RPA to stabilize and protect the ssDNA from premature degradation (Figure 4a). Through the direct interaction between ATRIP, which is associated with ATR, and ssDNA-bound RPA, ATR is localized to sites of replication stress or DNA damage. RPA additionally interacts with RAD17 and thereby recruits the ring shaped DNA damage-specific RAD9, RAD1, HUS1 complex (also called 9-1-1), which binds at junctions between ssDNA and double-strand DNA (Figure 4b). The 9-1-1 complex then recruits TOPBP1, which is thought to be the critical step in ATR activation. Activated ATR participates in DNA repair mechanisms by targeting the Fanconi anemia proteins FANCD2 and FANCI (comprehensively reviewed by Nepal *et al.* [66]), and also by phosphorylating the HR

regulatory protein BRCA1 (Figure 4c). The primary phosphorylation target of ATR, however, is the kinase CHK1, for whose phosphorylation and thereby activation Claspin is necessary. Activated CHK1 acts as intermediary, and induces various reactions including DNA repair, cell cycle checkpoint activation, or replication origin firing (Figure 4d). In regard to DNA repair, CHK1 recruits and phosphorylates the HR proteins RAD51 and BRCA2. By targeting Wee1 together with Cdc25A, or Cdc25C, CHK1 is able to induce S-phase, or G_2/M arrest, respectively, and thus mediates cell cycle checkpoint activation. Additionally, the inhibition of replication origin firing and thus the reduction of DNA replication rate under replication stress or DNA damaging conditions appears to be related to the initiation and maintenance of the S-phase arrest by CHK1 [4, 53, 84].

From a clinical perspective, the ATR pathway evolved as a promising target in cancer therapy. As ATR pathway inhibitors were demonstrated to effectively eliminate certain subsets of cancer cells [31, 98], several ATR [47, 78] and also CHK1 inhibitors [19, 89, 99] are currently investigated in clinical trials. Although the specific determinants of this therapeutic response are only insufficiently defined, it is likely to be at least partly attributable to synthetic lethal relationships between *ATR* and other DNA repair/genome maintenance genes. Thus, such synthetic lethal interactions with *ATR* should be comprehensively identified and characterized with particular regard to polymerases.

1.5 Previous data and aims of this project

In a previous study from our laboratory, Hocke *et al.* [41] identified synthetic lethal partners of *ATR*. Therefore, they used a small interfering RNA (siRNA) library targeting 288 DNA repair genes in a cellular *ATR*-knock-in model, which consisted of *ATR*-proficient $ATR^{+/+}$ and *ATR*-deficient $ATR^{s/s}$ cells, of the colorectal cancer (CRC) cell line DLD-1. By comparing the proliferation inhibitory effects on both $ATR^{+/+}$ and $ATR^{s/s}$ cells upon transfection with the respective siRNA, Hocke *et al.* [41] were able to identify genes whose depletion induced an *ATR*-dependent proliferation inhibition. Consequently, these genes represented potential synthetic lethal partners of *ATR*. *POLD1*, the catalytic subunit of Polδ, showed the strongest proliferation inhibitory effects among those identified genes. Thus, the work of Hocke *et al.* [41] started to additionally characterize the synthetic lethal relationship between *ATR* and *POLD1*. They showed that synthetic lethality and concomitantly the proliferation inhibitory effects were inducible upon both genetic and chemical inhibition of the ATR pathway in siRNA-mediated *POLD1*-depleted DLD-1 cells and various other CRC cell lines. Mechanistically, they observed that *POLD1*-depletion in *ATR*-deficient cells did not impair cell cycle progression, but caused caspase-dependent

apoptosis and increased DNA damage along with impaired DNA repair. In addition, the synthetic lethal relationship between *ATR* and *POLD1* [41] could have direct clinical relevance, as multiple *POLD1* VUS were recently reported in colorectal and other cancers, however, with unknown significance to act as potential biomarkers for a targeted therapy with ATR pathway inhibitors [7, 74, 94]. The knowledge and correct interpretation of such VUS is important especially for clinics and physicians, as demonstrated by the example of *BRCA1/2* VUS, whose identification might influence important surgical decision-making for women [100]. Furthermore, the previous screen also identified *PRIM1*, the catalytic subunit of primase of the Polα-primase complex, as one potential synthetic lethal partner of *ATR*, inducing the second strongest proliferation inhibitory effects upon inactivation of *ATR*. Thus, this dissertation was divided into two subprojects to investigate the synthetic lethal relationships between *ATR* and DNA polymerases, namely *PRIM1* and *POLD1* as catalytic subunits of the Polα-primase complex and Polδ, respectively.

The first subproject aimed to characterize the synthetic lethal relationship between *ATR* and *PRIM1*, analogous to the characterization of the synthetic lethal relationship between *ATR* and *POLD1* by Hocke *et al.* [41], by addressing the following questions:

- is the previously observed synthetic lethal relationship between *ATR* and *PRIM1* verifiable?
- are the observations specific, or the result of clonal artifacts of the genetically engineered *ATR*-knock-in model, or off-target effects of the siRNA targeting *PRIM1* (*siPRIM1*), respectively?
- is the proliferation inhibition also inducible in *siPRIM1*-transfected *ATR*-proficient cells upon treatment with clinically relevant ATR pathway inhibitors?
- is this synthetic lethal relationship between *ATR* and *PRIM1* also reproducible in other cell lines derived from different tumor entities?
- which molecular mechanism underlies the synthetic lethal relationship between *ATR* and *PRIM1*?

The second subproject aimed to characterize the impact of specific *POLD1* VUS on the sensitivity of cancer cells to treatment with ATR pathway inhibitors. Therefore, we used the CRISPR/Cas9 technique to establish a cellular *POLD1*-knockout (KO) model in the CRC cell line DLD-1, which harbors four heterozygous *POLD1* VUS [28]. Subsequently, this model was used to answer the following questions:

- do specific *POLD1* VUS have an impact on *POLD1* gene function and ATR pathway activation?

- which *POLD1* VUS increase the sensitivity of cancer cells to ATR pathway inhibitors *in vitro*?
- which *POLD1* VUS increase the sensitivity of cancer cells to ATR pathway inhibitors *in vivo*?

2 Methods

2.1 Cell culture

Thawing Frozen cells were removed from liquid nitrogen storage, shortly thawed at 37 °C, and added to their cultivation medium. The cell suspension was centrifuged at 300 g for 5 minutes, and the cell pellet was re-suspended in 1 ml cultivation medium, subsequently added to an appropriate amount of cultivation medium in a culture flask, and stored at 37 °C and 5 % CO_2. The following day, non-adherent cells were removed by replacing the medium with fresh cultivation medium.

Cultivation Cells with a confluence of 90 % were split by removing the cultivation medium, washing with phosphate buffered saline (PBS), and detaching by using 0.05 % Trypsin-EDTA for 5 minutes at 37 °C. Detachment was stopped by adding cultivation medium twice of the amount of used Trypsin-EDTA. Cell suspension was added in a ratio of 1:4 to 1:10 to a new culture flask with an appropriate amount of cultivation medium. The splitting procedure was performed twice a week, and cell culture flasks were stored at 37 °C and 5 % CO_2.

Freezing Detached cells were centrifuged at 300 g for 5 minutes. At least 1×10^6 cells were re-suspended in 1 ml cultivation medium supplemented with 10 % dimethyl sulfoxide (DMSO), and transferred to cryovials, which were primarily stored by using a freezing container at -80 °C to achieve a cooling rate of -1 °C/minute. The following day, cryovials were transferred to liquid nitrogen for permanent storage.

2.2 Transfection

The permanent or temporary introduction of foreign genetic material into eukaryotic cells is called transfection. For this, a reverse liposome transfection was used by enclosing the genetic material with the cationic, phospholipid-based transfection reagent, forming vesicles that can merge with the cell membrane and hence introducing the genetic material into the cells.

Plasmid DNA (1 µg) or siRNA (10 nM) were mixed with the 0.5-fold amount of the transfection reagent HiPerFect instead of the amount recommended by the manufacturer. To allow stable formation of transfection complexes, the genetic material and HiPerFect were incubated in medium free of fetal bovine serum (FBS) for 20 minutes at room temperature (RT). In the meantime, the appropriate cell number was prepared and seeded in wells required for the respective assays. Transfection complexes were added directly after their formation to the freshly seeded cell suspension and incubated at 37 °C and 5 % CO_2 for the required time period.

2.3 Establishment of an *ATR* re-expressing cell clone

ATR-deficient $ATR^{s/s}$ cells were seeded in 6-well plates and co-transfected as described with vectors pcDNA3-ATR WT, conferring neomycin resistance, and pLKO-U6-Tet-on-shNT5E-965, conferring puromycin resistance, in a ratio of 10:1. The co-transfection was necessary, as $ATR^{s/s}$ cells already harbor a neomycin resistance [42]. The transfection complex containing cultivation medium was replaced with puromycin containing cultivation medium for selection of stably transfected cells. After three weeks of selection, selected cells were allowed to grow in single cells colonies for two weeks, and consecutively screened by immunoblotting for high expression of ATR as compared to $ATR^{s/s}$ cells. The clone with the highest expression of ATR was chosen for further experiments.

2.4 Western blot

Total protein extraction Cells were centrifuged at 300 g for 5 minutes, the supernatant was discharged, and the pellet re-suspended and incubated for 20 minutes in lysis buffer, containing the two phosphatase inhibitors Na_3VO_4 and phenylmethylsulfonyl fluoride (PMSF) as well as the protease inhibitor "ProteaseArrest". The suspension was centrifuged at 10 000 rpm for 2 minutes, and the supernatant was used in a Bradford protein assay to determine the protein concentration. This assay contained Coomas sie Brilliant Blue G-250, a red dye that turns into a blue state after

complexing with proteins. The blue intensity was photometrically analyzed, and protein concentration was estimated by using a straight calibration line of bovine serum albumin (BSA). Finally, dithiothreitol (DTT) at a final concentration of 0.1 M, and sodium dodecyl sulfate (SDS) loading buffer were added to the protein lysate to break disulfide bridges and to denature proteins to their linear shape, as this structure is necessary for the subsequent electrophoretic migration.

Immunoblotting Empty buffer was added to the protein samples to reach an equivalent volume for each sample, before they were heated for 5 minutes at 95 °C. Samples were loaded on polyacrylamide gels in running buffer and allowed to electrophoretically migrate through the gels. After separation, proteins were transferred to a polyvinylidene fluoride (PVDF) membrane with the tank blot technique and transfer buffer. To avoid unspecific binding of antibodies, the blotted membrane was blocked with blocking buffer for 1 hour at RT, and then incubated overnight at 4 °C in fresh blocking buffer, containing the primary antibody directed against the target protein (Table 6). The antibody solution was removed, and the membrane was washed with TBST, incubated for 1 hour at RT in fresh blocking buffer containing a horseradish peroxidase (HRP) conjugated secondary antibody (Table 7) targeted against the primary antibody, and subsequently washed. By treating the membrane with a substrate containing luminol, which is oxidated by the HRP conjugated secondary antibody, a chemiluminescence reaction was induced and detected by a ChemoCam. The intensity of the chemiluminescence signals correlated with the protein amount and hence was used to detect and quantify proteins. Afterwards, the membrane was incubated for 1 hour at RT in blocking buffer containing a HRP conjugated antibody targeting β-Actin, serving as loading control to ensure the protein amounts of all loaded samples to be equivalent. Finally, the membrane was washed and the amount of β-Actin was detected and quantified using the luminol containing substrate as described above.

2.5 Cell proliferation assay

Cell proliferation assays were used to quantify the amount of surviving cells after treatment with various drugs at multiple concentrations. Depending on the experimental design, one of the following three procedures was conducted: cells were seeded in 96-well plates (600 $ATR^{+/+}$ and $ATR^{s/s}$ cells each, 800 ATR^{resc} cells, 1800 $POLD1^{+/+}$, $POLD1^{+/+}$ control (ctrl), and $POLD1^{R689W/-}$ cells each, or 1500 $POLD1^{+/-}$ cells) and treated the following day with the respective drug for 120 hours; cells were seeded in 96-well plates (600 $ATR^{+/+}$ and $ATR^{s/s}$ cells each, or 800 ATR^{resc} cells) and transfected as described for 144 hours; cells were seeded in 6-well plates (1×10^5

DLD-1 and SW480 cells each, 7×10^4 RKO cells, or 6.6×10^4 PaTu 8988t cells) and transfected as described for 96 hours before transfected cells were transferred to 96-well plates (600 DLD-1 cells, 1000 SW480 cells, 800 mock-transfected cells and non-transfected cells (NTC) of RKO and PaTu 8988t each, or 2000 *siPRIM1*-transfected cells of RKO and PaTu 8988T each) and treated the following day with the respective drug for 120 hours. Following each incubation period at 5 % CO_2 and 37 °C, medium was removed, and cells were washed with PBS and lysed for 30 minutes with H_2O supplemented with 0.2 % SYBR® Green I, which intercalated with the DNA of lysed cells. In this state it emitted a green fluorescent dye that was detected by a plate reader. The amount of fluorescent signals correlated with the amount of cells in each well. The surviving fraction was calculated as compared to untreated control samples.

2.6 Flow cytometry

Flow cytometry allows the characterization of certain cell populations by optically analyzing single cells, which are labeled with fluorochrome conjugated antibodies. Light emitted in this way is detected and quantified, allowing the identification and analysis of cell populations within a heterogeneous cell suspension. For this work, flow cytometry was used to analyze the cell cycle profile.

Cells were seeded and transfected as described in 6-well plates. After 144 hours, cells were collected, washed in PBS, and centrifuged at 300 g for 5 minutes. The cell pellet was re-suspended in a PI staining solution and incubated at 4 °C overnight as previously described [68]. The cell cycle distribution was quantified by using a flow cytometer. At least 20 000 gated events per sample were analyzed with the FlowJo software.

2.7 Immunocytochemistry

Immunocytochemistry is a technique to microscopically assess cellular structures, visualized by fluorochrome conjugated antibodies targeting the respective proteins. For this dissertation, nuclear focus formation at sites of DNA damage was analyzed. Cells were seeded and transfected as described on sterile coverslips in 6-well plates. After incubation for 120 hours, the cultivation medium was removed, and cells were washed with PBS and fixed with 3.7 % formaldehyde for 10 minutes. After a short incubation in ice-cold methanol (-20 °C), cells were washed in PBS for 5 minutes, incubated in permeabilization solution for 10 minutes, and afterwards in blocking solution for 30 minutes. The primary antibody (Table 6), diluted in blocking solution, was applied overnight at 4 °C. Cells were washed in blocking solution three times for

5 minutes, before secondary antibody (Table 7), diluted in blocking solution and conjugated with a fluorochrome, was applied for 2 hours at RT. Then, slides were washed with blocking solution three times for 5 minutes and mounted on object slides, using a mounting medium supplemented with 4',6-diamidino-2-phenylindole (DAPI), a fluorescent DNA stain. Object slides were microscopically analyzed, and focus formation of at least 70 cells was quantified using the ImageJ software.

2.8 Gene knockout with CRISPR/Cas9

CRISPR/Cas9 is part of the prokaryotic immune system to confer resistance to foreign genetic material, and is also basis of a molecular biological technique that enables a highly specific and easy to achieve genome editing. The Cas9 endonuclease (Figure 17) is associated with a guide RNA (gRNA), which harbors a sequence targeting the gene of interest. It binds a protospacer adjacent motif (PAM), and—if the gRNA sequence hybridizes perfectly with the target DNA sequence—introduces a DSB upstream the PAM. This DSB can either be repaired by non-homologous end joining via introducing indel mutations, or by HR. The latter repair mechanism introduces specific sequences into the genome if a repair template is provided. Also, a repair template allows to generate a gene KO by disrupting the Cas9-binded exon structure.

For this project, a CRISPR/Cas9 *POLD1* knockout kit was used, containing two Cas9 plasmids (targeted sequence of gRNA1 TGCCCCCAAAGCGGGCCCGT and gRNA2 GGGATGATGATGATGCACCT, respectively), one Cas9 plasmid with a scrambled sequence as control and a repair template with a floxed puromycin resistance gene together with a left homology arm (LHA) and right homology arm (RHA) region (Figure 18). In exon 2a of the *POLD1* locus Cas9 induced a DSB, allowing the integration of the repair template due to the LHA and RHA regions. This repair template was used to repair the DSB via HR, resulting in a disrupture of *POLD1*, and thus causing a KO (Figure 5).

Cells were seeded in 6-well plates and co-transfected as described with one of the three Cas9 plasmids and the repair template for 72 hours. The transfection complex containing medium was replaced with puromycin containing medium for selection of stably transfected cells. Selected cells were allowed to grow in single cell colonies for two weeks and genotyped, using the primers #1–#4 (Table 8). Heterozygous clones show two PCR products, one representing the KO allele (~1000 bp) and the other one representing the intact wild type (WT) allele (1656 bp). To engineer homozygous KO clones, heterozygous clones were first transfected with a Cre vector for 72 hours to remove the floxed puromycin resistance (PuroR) gene. Single cell colonies with removed PuroR gene were genotyped using primers #5 and #6 (Table 8).

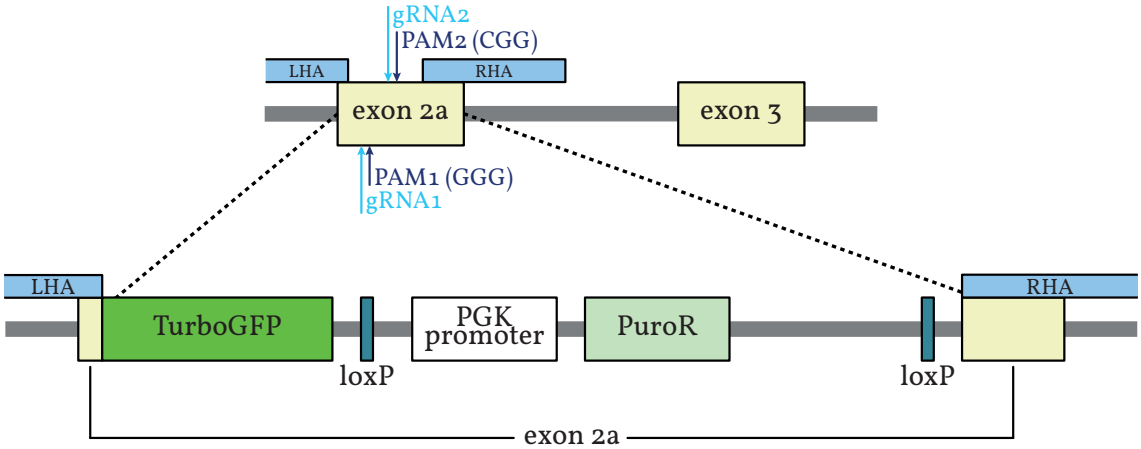

Figure 5 | Disruption of *POLD1* exon 2a by integrating a repair template
Schematic overview of the targeting procedure, displaying CRISPR/Cas9-mediated integration of the repair template in exon 2a of the *POLD1* locus. **Abbreviations** | gRNA: guide RNA; LHA: left homology arm; PAM: protospacer adjacent motif; PuroR: puromycin resistance; RHA: right homology arm.

Colonies without the PuroR gene were transfected again with one of the three Cas9 plasmids, and the repair template as described.

2.9 Polymerase chain reaction

Preparation of genetic templates RNA or DNA was isolated from cells, following the manufacturer's instructions of the RNA/DNA purification kits, and concentrations were measured using a nano drop. For amplification, RNA was reverse transcribed into complementary DNA (cDNA), using a reverse transcription kit. A mastermix was prepared, including 1× buffer, mix of deoxyribonucleotide triphosphate (dNTP) (each 1 mM), 0.2 µM oligo(dT) primer, 2 units of reverse transcriptase, and 0.5–1 µg RNA per reaction, added to RNase-free water. The reverse transcription mix was incubated at 37 °C for 1–2 hours.

Amplification and gel electrophoresis Genomic DNA or newly synthesized cDNA served as template for the amplification of the DNA fragments of interest. A mastermix was prepared, including 1× buffer, mix of dNTP (each 0.2 mM), forward and reverse primer (each 0.5 pmol, Table 8), 1.25 units of *Taq* polymerase, and 100–200 ng DNA template per reaction, added to nuclease-free water. After amplification in a thermal cycler (all PCR programs and conditions are described in the appendix, Figure 19 and Table 10), 1× DNA loading dye was added to the PCR mix. For electrophoretic separation, samples were loaded on a 1 % agarose gel (prepared in TBE buffer) supplemented with a UV sensitive dye, that intercalated with DNA and hence visualized the amplified PCR products on a UV transilluminator.

Sequencing Sequencing of the amplified DNA was performed by GATC Biotech, utilizing Sanger's chain-termination method. Normal dNTPs together with dideoxyribonucleotide triphosphates (ddNTPs), of which each was conjugated with a different fluorochrome, were used in a PCR-similar reaction. Whenever a ddNTP instead of a dNTP was used by the polymerase, the elongation of the DNA strand terminated, leaving DNA fragments of different sizes, each of them with a certain terminal fluorescent signal. Arranged by size via capillary gel electrophoresis, a laser detected the fluorochomes and depicted all fluorescent signals in a chromatograph, allowing computational sequence analysis. Samples were prepared as asked by GATC Biotech, and sequencing primers are listed in Table 8.

2.10 DNA fiber assay

The DNA fiber assay is a technique to analyze the replication process by microscopically quantifying length and structure of single DNA fibers. These experiments were kindly performed by Prof. Dr. Kerstin Borgmann and Alexandra Zielinski from the Lab of Radiobiology & Experimental Radiooncology of the University Medical Center Hamburg-Eppendorf in Hamburg.

Exponentially growing cells were labeled with 25 µM 5-chloro-2′-deoxyuridine (CldU) followed by 250 µM 5-iodo-2′-deoxyuridine (IdU) for 30 minutes each. For analysis of fork stability, cells were treated with 2 mM hydroxyurea (HU) for 4 hours, or irradiated with 6 Gy between both labels. Labeled cells were harvested, and their DNA fiber spreads were prepared and stained as previously described [69, 75]. In short, labeled cell suspension was placed on object slides and lysed, before object slides were tilted 15°, allowing DNA fibers to spread. After air drying DNA fibers were fixed and denatured with HCl, before incubated in primary antibodies. A monoclonal rat anti-BrdU antibody was used to detect CldU, and a monoclonal mouse anti-BrdU was used to detect IdU. Goat anti-rat and goat anti-mouse antibodies — conjugated with AlexaFluor 555 or AlexaFluor 488, respectively — were used as secondary antibodies, and DNA fibers were examined using an Axioplan 2 fluorescence microscope. CldU and IdU tracks were measured, using the ImageJ software, and micrometer values were converted into kilobases. At least 100 forks were analyzed. Different classes of labeled tracks were classified: red-green (ongoing replication), red (stalled forks), and green (2^{nd} pulse origins). Labeled tracks were counted using the ImageJ software, and at least three independent experiments were performed.

2.11 Mouse xenograft tumor model for *in vivo* experiments

The mouse xenograft tumor model enables the analysis of the impact of pharmaceutical drugs on induced tumors in a living organism. As tumors are induced by cells of different species, a strong immunological reaction would normally be provoked in mice. To avoid this, mice with a genetically induced athymic phenotype and a subsequent strong decrease of T cells are used.

To calculate the required group size we used 5 % for the error of the first kind and 0.9 for the statistical power, resulting in an effect size of 1.5 with estimated tumor volumes of 1200 mm^3 for the control group, 900 mm^3 for the treatment group, and an estimated standard deviation of 200 mm^3. According to G*Power — a program recommended by the regional commission of Gießen to calculate the group size — these values resulted in a size of nine mice per group. All animal experiments were performed according to the guidelines of the German law for animal life protection and approved by the regional commission of Gießen with the file number G44/2017.

Four week old female NMRI-*Foxn1*$^{nu/nu}$ nude mice were purchased and allowed to acclimate for two weeks in an incubator with constant temperature and humidity. Xenograft tumors were induced by subcutaneously injecting 10^6 cells of DLD-1 *POLD1*$^{+/+}$ or *POLD1*$^{R689W/-}$ cells, respectively, both suspended in PBS. Two weeks after injection mice with a palpable tumor were randomly divided into two groups for each cell clone and the ATR inhibitor AZD6738 at a dose of 50 mg/kg or the vehicle solution alone were administered by gavage once daily for five consecutive days, followed by two days of no administration. This application schedule was conducted for four weeks (Figure 6), as long as the immediate no-go criteria, i. e. a tumor diameter of ≥1.5 cm, or a loss of body weight of ≥20 % (equivalent to a body condition score of 1), were not met. During this period, mice were weighed and scored for their body condition daily. Furthermore, the tumor size was measured twice a week with

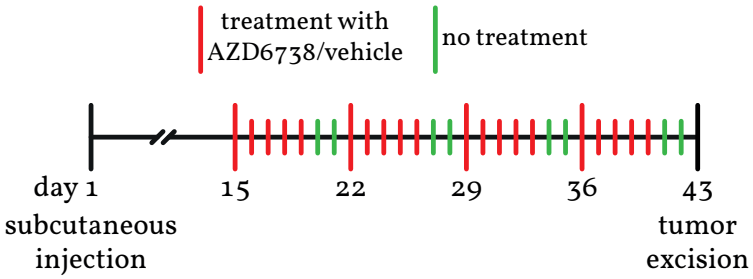

Figure 6 | Schematic depiction of the application schedule
Cancer cells were subcutaneously injected on day 1, and allowed to grow for two weeks. Starting on day 15, mice were treated either with AZD6738 or with vehicle for five consecutive days, followed by two days without treatment. This application schedule was conducted for four weeks before on day 43 tumors were excised.

calipers and the calculated tumor volume ($V = x \cdot y^2 \cdot 0.5$, with x = longest diameter, y = shortest diameter) on day one of the inhibitor/vehicle application was set as reference to calculate the percentage change of tumor volume.

2.12 Statistical analyses

All statistical analyses were performed using Prism 5, and data are presented as mean ± SD. Surviving fractions of proliferation assays were calculated by curve fitting with nonlinear regression. A two-tailed, unpaired Student's t test or a two-way ANOVA with Bonferroni post-test were used for statistical interpretation. P values of $P < 0.05$ (*), $P < 0.01$ (**), or $P < 0.001$ (***) were considered statistically significant.

3 Material

3.1 Cell lines and other organisms

The human CRC cell lines DLD-1, SW-480, and RKO were purchased from the Leibniz Institute DSMZ (Braunschweig, Germany) or the American Type Culture Collection (LGC Standards, Wesel, Germany). The human pancreatic cancer cell line PaTu 8988t was kindly provided by Hans-Peter Elsässer (Philipps-University Marburg, Germany). The DLD-1 cell clone ATR$^{s/s}$ was kindly provided by Fred Bunz (John Hopkins University, Baltimore, MD, USA), and has been characterized previously [30, 31, 42]. NMRI*Foxn1*$^{nu/nu}$ nude mice were purchased from Charles River Laboratories (Wilmington, MA, USA).

3.2 Equipment, software, and expendable materials

Table 1 | Equipment

Equipment	Company
Air flow cabinet (Uniprotect)	EHRET Labor- und Pharmatechnik
Balance (EMB 500-1)	KERN & SOHN
Biological safety cabinets (MSC-Advantage™)	Thermo Fisher Scientific
Biosafety changing station (interACTIVE)	Tecniplast
Centrifuge (Heraeus™ Megafuge™ 8)	Thermo Fisher Scientific

Table 1 | Equipment (continued)

Equipment	Company
Centrifuge (Heraeus™ Multifuge 3SR+)	Thermo Fisher Scientific
Centrifuge (Micro Star 17)	VWR
ChemoCam	INTAS Science Imaging Instruments
Feeding tube, 20 ga×38 mm	Instech Laboratories
Flow cytometer (BD FACSCanto II)	BD Biosciences
Freezer -80 °C (HERAfreeze™)	Thermo Fisher Scientific
Freezing container (Nalgene® Mr. Frosty)	Sigma-Aldrich
Incubation bath	GFL
Incubator (Heracell™ 240i)	Thermo Fisher Scientific
Microplate photometer (Multiskan FC)	Thermo Fisher Scientific
Microscope (Axioplan 2)	Carl Zeiss
Microscope (Axiovert 200M)	Carl Zeiss
Microscope	Olympus
Multichannel pipette (Pipet-Lite XLS L-300)	Mettler-Toledo
Nano drop ND-1000	Peqlab Biotechnologie
Neubauer chamber	Plan Optik
Pipetboy	INTEGRA Biosciences
Pipettes	Gilson
Plate reader (Victor³ V)	PerkinElmer
Refrigerator -20 °C, 4 °C	Liebherr
Thermal cycler (T100™ Thermal Cycler)	Bio-Rad Laboratories
Thermomixer 5436	Eppendorf
UV transilluminator	Intas Science Imaging Instruments

Table 2 | Software

Software	Company
Creative Suite 5	Adobe Systems
FlowJo v10	FlowJo
GraphPad Prism 5	GraphPad Software

Table 2 | Software (continued)

Software	Company
ImageJ 1.49v	Wayne Rasband, National Institutes of Health, USA
Mendeley Desktop v1.17.13	Mendeley
MiKTEX 2.9	Christian Schenk
Office 2013	Microsoft
SnapGene® Viewer v4.1.4	GSL Biotech
TEXworks v0.6.2	Jonathan Kew, Stefan Löffler, Charlie Sharpsteen

Table 3 | Expendable material

Expendable materials	Company
6-well plate	Greiner Bio-One
96-well plate F-bottom	Greiner Bio-One
Cell culture flask (T25, T75)	Sarstedt
Coverslips (Menzel-Gläser 24 × 24 mm)	Thermo Fisher Scientific
Cryotubes (Cryo.s™)	Greiner Bio-One
Microtest Plate 96-well, F	Sarstedt
Object slides (Superfrost®Plus)	Thermo Fisher Scientific
Pipette tips (1000 µl)	Sarstedt
Pipette tips (10 µl, 200 µl)	Sarstedt
Pipette tips (multichannel pipette)	Mettler-Toledo
PVDF membrane (Immobilon®-P transfer membrane)	Merck
Reaction tubes (0.5 ml, 1.5 ml, 2 ml)	Sarstedt
Reaction tubes (15 ml, 50 ml)	Sarstedt
Reaction tubes PCR (Multiply-Pro cup 0.2 ml)	Sarstedt
Serological pipettes (2 ml)	Greiner Bio-One
Serological pipettes (5 ml, 10 ml, 25 ml, 50 ml)	Sarstedt
Syringe 1 ml (NORM-JECT®)	Henke-Sass, Wolf
Tube 5 ml, 75 × 12 mm, PS	Sarstedt

3.3 Chemicals, reagents, solutions, and media

Table 4 | Chemicals and reagents

Substance	Company
1,2-Bis(dimethylamino)ethane (TEMED)	Sigma-Aldrich
1,3-Propanediol	Sigma-Aldrich
4-(2-Hydroxyethyl)piperazine-1-ethanesulfonic acid (HEPES)	Carl Roth
5-Chloro-2′-deoxyuridine (CldU)	Sigma-Aldrich
5-Fluorouracil (5-FU)	Sigma-Aldrich
5-Iodo-2′-deoxyuridine (IdU)	Sigma-Aldrich
Acrylamide (Rothiphorese® Gel 30)	Carl Roth
Agarose	Carl Roth
Ammonium persulfate (APS)	Sigma-Aldrich
Aqua dest.	B. Braun
AZD6738 (*in vitro*)	MedKoo Biosciences
AZD6738 (*in vivo*)	AdooQ Bioscience
Boric acid	Carl Roth
Bovine serum albumin (BSA)	Thermo Fisher Scientific
Bradford solution (Roti®-Nanoquant)	Carl Roth
Bromophenol blue	Sigma-Aldrich
Carboplatin	University Hospital Marburg
Cre vector	Santa Cruz Biotechnology
CRISPR/Cas9 genome knockout kit	OriGene Technologies
Deoxyribonucleotide triphosphate (dNTP) mix	Thermo Fisher Scientific
Dimethyl sulfoxide (DMSO)	Carl Roth
Dithiothreitol (DTT)	SERVA Electrophoresis
DNA gel loading dye	Thermo Fisher Scientific
DNA ladder (GeneRuler 1 kb)	Thermo Fisher Scientific
DNA purification kit (QIAmp® DNA Mini Kit)	Qiagen
Ethylene glycol-bis(2-aminoethylether)-N,N,N′,N′-tetraacetic acid (EGTA)	Sigma-Aldrich
Ethylenediaminetetraacetic acid (EDTA)	Sigma-Aldrich

Table 4 | Chemicals and reagents (continued)

Substance	Company
Fetal bovine serum (FBS)	Thermo Fisher Scientific
Formaldehyde 3.7 %	Otto Fischar
Glycerol	Carl Roth
HiPerFect	Qiagen
Hydroxyurea (HU)	Sigma-Aldrich
Luminol substrate (Clarity™ Western ECL substrate)	Bio-Rad Laboratories
Luminol substrate (Western Lightning® Ultra)	PerkinElmer
LY2603618	Selleckchem
Methanol	Sigma-Aldrich
MK-8776	Selleckchem
Mounting medium (Roti®-Mount FluorCare DAPI)	Carl Roth
Mytomycin C (MMC)	Sigma-Aldrich
Na_3VO_4	Sigma-Aldrich
$Na_4P_2O_7 \cdot 10\ H_2O$	Sigma-Aldrich
NaCl	Carl Roth
NaF	Sigma-Aldrich
Oligo(dT) primer	biomers
Oxaliplatin	University Hospital Marburg
Phenylmethylsulfonyl fluoride (PMSF)	Sigmal-Aldrich
Phosphate buffered saline (PBS)	Thermo Fisher Scientific
Polymerase (GoTaq® G2 DNA Polymerase)	Promega
Powdered milk	Carl Roth
Primer (PCR/sequencing)	biomers/GATC Biotech
Propidium iodide (PI)	Sigma-Aldrich
Protease inhibitor (ProteaseArrest)	G-Bioscience
Protein ladder (PageRuler™)	Thermo Fisher Scientific
Protein ladder (Spectra™ multicolor high range)	Thermo Fisher Scientific
Puromycin	InvivoGen

Table 4 | Chemicals and reagents (continued)

Substance	Company
Reverse transcription kit (Omniscript® RT Kit)	Qiagen
RNA purification kit (RNeasy® Mini Kit)	Qiagen
RPMI 1640	Thermo Fisher Scientific
siPOLD1 (5'-CGGGACCAGGGAGAATTAATA-3')	Qiagen
siPRIM1 (5'-AACCACAGATCAAATACTTCA-3')	Qiagen
Sodium citrate	Sigma-Aldrich
Sodium dodecyl sulfate (SDS)	Carl Roth
SYBR®Green I	Lonza
Tris	Carl Roth
Triton X-100	Carl Roth
Trypsin	Thermo Fisher Scientific
Tween 20	Sigma-Aldrich
UV sensitive dye (HDGreen Plus DNA Stain)	Intas Science Imaging Instruments
VE-822	MedKoo Biosciences
Vector pcDNA3-ATR WT	Addgene (donated by Aziz Sancar [45])
Vector pLKO-U6-Tet-on-shNT5E-965	Stephan A. Hahn, Laboratory of Molecular Oncology, University Bochum, Germany

Table 5 | Media, buffer, and solutions

Medium	Ingredient	Concentration
Blocking buffer	Powdered milk	5 %
	TBST	pure
Blocking solution	BSA	2 %
	Permeabilization solution	pure
Cultivation medium	FBS	10 %
	RPMI 1640	pure

Table 5 | Media, buffer, and solutions (continued)

Medium	Ingredient	Concentration
Empty buffer	PBS	70 %
	SDS loading buffer	30 %
Lysis buffer	EGTA	1 mM
	Glycerol	10 %
	HEPES	50 mM
	Na_3VO_4	2 mM
	$Na_4P_2O_7 \cdot 10\,H_2O$	10 mM
	NaCl	150 mM
	NaF	100 mM
	PMSF	1 mM
	ProteaseArrest™	1 %
	Triton X-100	1 %
Permeabilization solution	TBS	pure
	Triton X-100	0.5 %
PI staining solution	Propidium iodide	50 µg/ml
	Sodium citrate	0.1 %
	Triton X-100	0.1 %
Running buffer	Glycine	190 mM
	Tris	25 mM
	SDS	0.1 %
SDS loading buffer, pH 6.8	Bromophenol blue	1.9 mM
	Glycerol	40 %
	H_2O	50 %
	SDS	0.5 %
	Tris	63 nM
Separating gel buffer, pH 8.8	SDS	0.4 %
	Tris	1.5 M
Separating gel solution, 10 %	Acrylamide	33 %
	APS	0.02 %
	H_2O	pure
	Separating gel buffer	25 %
	TEMED	0.2 %

Table 5 | Media, buffer, and solutions (continued)

Medium	Ingredient	Concentration
Stacking gel buffer, pH 6.8	SDS	0.4 %
	Tris	0.5 M
Stacking gel solution	Acrylamide	4.8 %
	APS	0.03 %
	H_2O	pure
	Stacking gel buffer	25 %
	TEMED	0.3 %
TBE buffer	Boric acid	89 mM
	EDTA	2 mM
	Tris	89 mM
TBS buffer, pH 7.6	NaCl	150 mM
	Tris	20 mM
TBST buffer, pH 7.6	TBS	pure
	Tween 20	0.1 %
Transfer buffer, pH 8.3	Glycine	190 mM
	Tris	20 mM
	SDS	0.1 %
Vehicle solution	1,3-propanediol	40 %
	DMSO	10 %
	H_2O	50 %

3.4 Antibodies and primer

Table 6 | Primary antibodies

Target *(clone)*	Species	Dilution	Clonality	Company
ATR *(N-19)*	goat	1:500	poly	Santa Cruz Biotechnology
Caspase 3	rabbit	1:1000	poly	Cell Signaling Technology
Caspase 8 *(1C12)*	mouse	1:1000	mono	Cell Signaling Technology

Table 6 | Primary antibodies (continued)

Target *(clone)*	Species	Dilution	Clonality	Company
Caspase 9 *(H-170)*	rabbit	1:500	poly	Santa Cruz Biotechnology
Cdc25A *(5H51)*	mouse	1:1000	mono	Santa Cruz Biotechnology
CHK1 *(G4)*	mouse	1:500	mono	Santa Cruz Biotechnology
cleaved Caspase 3 (Asp175)	rabbit	1:1000	poly	Cell Signaling Technology
Cyclin A *(H-432)*	rabbit	1:1000	poly	Santa Cruz Biotechnology
PARP	rabbit	1:1000	poly	Cell Signaling Technology
pCHK1 (Ser345) *(133D3)*	rabbit	1:1000	mono	Cell Signaling Technology
POLD1 *(A-9)*	mouse	1:500	mono	Santa Cruz Biotechnology
PRIM1 *(8G10)*	rat	1:1000	mono	Cell Signaling Technology
Wee1 *(B-11)*	mouse	1:1000	mono	Santa Cruz Biotechnology
β-Actin (HRP conjugated) *(AC-15)*	mouse	1:40 000	mono	Sigma-Aldrich
γH2AX (Ser139) *(20E3)*	rabbit	1:200	mono	Cell Signaling Technology

Table 7 | Secondary antibodies

Target	Species	Conjugate	Dilution	Company
goat IgG	donkey	HRP	1:20 000	Santa Cruz Biotechnology
mouse IgG	bovine	HRP	1:10 000	Santa Cruz Biotechnology
rabbit IgG	goat	Alexa Fluor 488	1:500	Thermo Fisher Scienfitic

Table 7 | Secondary antibodies (continued)

Target	Species	Conjugate	Dilution	Company
rabbit IgG	goat	HRP	1:10 000	Santa Cruz Biotechnology
rat IgG	goat	HRP	1:10 000	Santa Cruz Biotechnology

Table 8 | Primer

Primer	Orientation	Localization	Sequence (5' - 3')
#1	forward	*POLD1*, upstream LHA[a]	GTGAGAGAGCACACACACGAC
#2	reverse	repair template, GFP	TAGGTGCCGAAGTGGTAGAAGC
#3	forward	repair template, spacer region	TCTCTTGATTCCCACTTTGTGGT
#4	reverse	*POLD1*, downstream RHA[b]	CAGATCAACGCTCCAAGCAC
#5	forward	repair template, LHA	GAGGTGTCTCCGGTCAGAAC
#6	reverse	repair template, PuroR[c]	GAGGCCTTCCATCTGTTGCT
#7	forward	*POLD1* NCS[d], upstream exon 13	CCCAGACCCTGACGACTTGG
#8	reverse	*POLD1* NCS, downstream exon 13	TGGGAGTGGGGAGAAAAAGTG
#9	forward	*POLD1* NCS, upstream exon 17	TGCGTGAATTAGCACAAGGC
#10	reverse	*POLD1* NCS, downstream exon 17	GGACCAATTGCTCAAGCCAC
#11	forward	*POLD1* NCS, upstream exon 18	TCCGCATGATTCTCTCCCCG
#12	reverse	*POLD1* NCS, downstream exon 18	GTGGCTAATGCCAACGGGAC
#13	forward	*POLD1*, exon 2a	GGGCCTCTGGGATGATGATG

Table 8 | Primer (continued)

Primer	Orientation	Localization	Sequence (5' - 3')
#14	reverse	*POLD1*, downstream exon 18	ACCGCATCGATATCTCCCAG
#15	forward	*POLD1*, upstream exon 13	GTATCATGGACCCCGACGTG
#16	reverse	*POLD1*, downstream exon 13	GCCCCTCAAAGGGTACTACG
#17	forward	*POLD1*, upstream exon 17	CTGTGTTACACCACGCTCCT
#18	reverse	*POLD1*, downstream exon 18	CAACCTGGTCACTGCCTCAC
#S1	forward	*POLD1* NCS, upstream exon 2a	TCAGAACCTCCACCAAG
#S2	forward	*POLD1* NCS, upstream exon 13	ACTTCCTTCTCCTGCTC
#S3	forward	*POLD1* NCS, upstream exon 17	TGTGCAGTGCACAGTAC
#S4	forward	*POLD1* NCS, upstream exon 18	GTTCGGACGTCAGATGATC
#S5	forward	*POLD1*, upstream exon 13	CTCCTACACGCTCAATG
#S6	forward	*POLD1*, upstream exon 17	AGATCCTGGAGAACCTG

[a] left homology arm
[b] right homology arm
[c] puromycin resistance
[d] non-coding sequence

4 Results

4.1 Characterizing the synthetic lethal relationship between *ATR* and *PRIM1*

The application of an siRNA library revealed a to date unknown synthetic lethal relationship between *ATR*, a central regulator of the DNA damage response, and *PRIM1*, the catalytic subunit of primase of the Polα-primase complex [41]. As therapy approaches based on synthetic lethal interactions gain in importance for an individualized and targeted treatment [55], the relationship between *ATR* and *PRIM1* could represent a novel concept for cancer therapy. Thus, the aim of this first subproject was to verify and further characterize the synthetic lethal relationship between *ATR* and *PRIM1*, assessing the impact of *PRIM1* depletion on cancer cells upon either genetic or chemical disruption of *ATR* function. In addition, we also investigated the underlying molecular mechanism regarding cell cycle progression and apoptosis.

4.1.1 Verifying the synthetic lethality of *ATR* and *PRIM1*

For the identification of the synthetic lethal relationship between *ATR* and *PRIM1* a well-defined *ATR* knock-in model was used [41], consisting of *ATR*-proficient ($ATR^{+/+}$) and *ATR*-deficient ($ATR^{s/s}$) cells of the human CRC cell line DLD-1 [42]. To exclude artifacts due to clonal variation of this *ATR* knock-in model we first established *ATR* re-expressing cells (ATR^{resc}) and confirmed the subtotal ATR protein depletion in $ATR^{s/s}$ and the ATR protein re-expression in ATR^{resc} cells via immunoblotting (Figure 7a). We confirmed the previously described increased sensitivity of

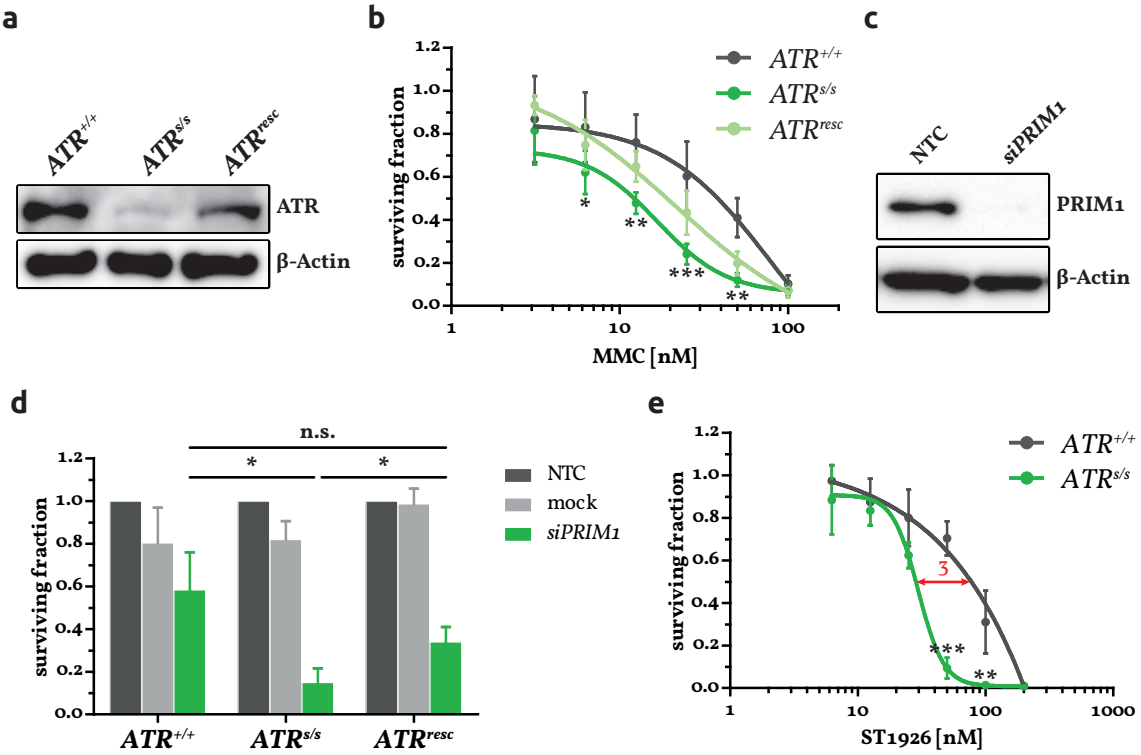

Figure 7 | Verification of the synthetic lethality between *ATR* and *PRIM1* in DLD-1 cells

a | ATR protein quantification in $ATR^{+/+}$, $ATR^{s/s}$, and ATR^{resc} cells via immunoblotting with β-Actin serving as loading control. **b** | MMC sensitivity assessment of $ATR^{+/+}$, $ATR^{s/s}$, and ATR^{resc} cells via proliferation assay 120 hours after treatment . **c** | PRIM1 protein quantification via immunoblotting 120 hours after *siPRIM1* transfection with β-Actin serving as loading control. **d** | Proliferation inhibition assessment of $ATR^{+/+}$, $ATR^{s/s}$, and ATR^{resc} cells via proliferation assay 144 hours after *siPRIM1* transfection. **e** | ST1926 sensitivity assessment of $ATR^{+/+}$ and $ATR^{s/s}$ cells via proliferation assay 120 hours after treatment. **Data information** | All data are presented as mean ± SD. Experiments were performed independently (n = 4 for figure part b; n = 3 for figure parts d + e) with each data point reflecting triplicate wells. Immunoblots were performed independently twice (figure part a) or three times (figure part c), respectively, and representative results are shown. Statistical significance (*$P < 0.05$, **$P < 0.01$, ***$P < 0.001$, n.s. = not significant) refers to *siPRIM1* vs. NTC if not depicted otherwise, and was calculated using a two-tailed, unpaired Student's *t* test (figure part d) or a two-way ANOVA with Bonferroni post-test (figure part b + e).

$ATR^{s/s}$ cells to ICL agents [30] by treatment with mitomycin C (MMC). This effect was partially reversible in ATR^{resc} cells (Figure 7b).

To verify the synthetic lethal relationship between *ATR* and *PRIM1* we depleted *PRIM1* in *ATR*-deficient cells by using an siRNA targeting *PRIM1* (*siPRIM1*, Figure 7c). Similarly to MMC, we confirmed the previously reported proliferation inhibition of $ATR^{s/s}$ cells upon *PRIM1* depletion [41] and observed partial rescue effects upon *ATR* re-expression (Figure 7d). To exclude off-target effects of *siPRIM1* we also assessed the sensitivity of $ATR^{s/s}$ cells to ST1926, a chemical inhibitor of Polα [1, 33, 37]. As there are no chemical inhibitors yet available to directly target primase, and primase is complexed with Polα, we thought a Polα inhibitor to be suitable to preliminarily

exclude off-target effects. In fact, we observed an increased sensitivity of $ATR^{s/s}$ cells to ST1926 as compared to $ATR^{+/+}$ cells with an IC_{50} ratio of 3 (Figure 7e).

In conclusion, by extending the well-defined *ATR* knock-in model with *ATR* re-expressing cells we excluded clonal variation, and verified the previously reported proliferation inhibitory effects on *ATR*-deficient cells either upon siRNA-mediated *PRIM1* depletion, or upon chemical Polα inhibition to be *ATR* specific.

4.1.2 Sensitizing various cancer cell lines to ATR and CHK1 inhibitors through *PRIM1* depletion

To assess a potential translational medical exploitability of the synthetic lethal relationship between *ATR* and *PRIM1* we analyzed whether the detrimental effects of *PRIM1* depletion on genetically induced *ATR*-deficient cells were similarly inducible in *ATR*-proficient cells upon chemical inhibition of ATR. Therefore, we treated $ATR^{+/+}$ NTC as well as mock- and *siPRIM1*-transfected DLD-1 cells (Figure 8a) with the selective and clinically investigated ATR inhibitors AZD6738 and VE-822 [47, 78]. The sensitivity of DLD-1 cells to treatment with these ATR inhibitors was significantly increased upon *PRIM1* depletion as compared to NTC with IC_{50} ratios of 14 and 9, respectively (Figure 8b). Additional treatment with the selective inhibitors LY2603618 and MK-8776 [19, 89, 99], targeting ATR's major downstream effector kinase CHK1, achieved similar effects with IC_{50} ratios of 9 and 10, respectively (Figure 8c). To exclude a general and unspecific drug hyper-sensitivity mediated by *PRIM1* depletion we treated cells with common chemotherapeutics including MMC, 5-fluorouracil (5-FU), and oxaliplatin, and observed no significant *PRIM1*-dependent effects (Figure 8d).

DLD-1 cells are known to be microsatellite-instable [3, 48]. Therefore, to exclude confounding artifacts, and at the same time to generalize our data beyond one single cell line we analyzed the effects of *PRIM1* depletion on additional cancer cell lines upon treatment with ATR and CHK1 inhibitors. We used NTC as well as mock- and *siPRIM1*-transfected cells of the human CRC cell lines SW480 and RKO, which are microsatellite-stable and -instable, respectively, as well as the human microsatellite-stable pancreatic cancer cell line PaTu 8988t [26] (Figure 9a). Similar to DLD-1 cells, we observed an increased sensitivity of SW480, RKO, and PaTu 8988t cells to treatment with ATR inhibitors (IC_{50} ratios ranging from 4 to at least 13, Figure 9b) and also CHK1 inhibitors (IC_{50} ratios ranging from 3 to at least 26, Figure 9c) upon *PRIM1* depletion as compared to NTC.

In summary, we showed that the detrimental proliferation inhibitory effects were also inducible in *ATR*-proficient cells using chemical inhibitors specifically targeting ATR and CHK1 independently of the microsatellite stability status, and applicable to multiple cell lines derived from different tumor entities.

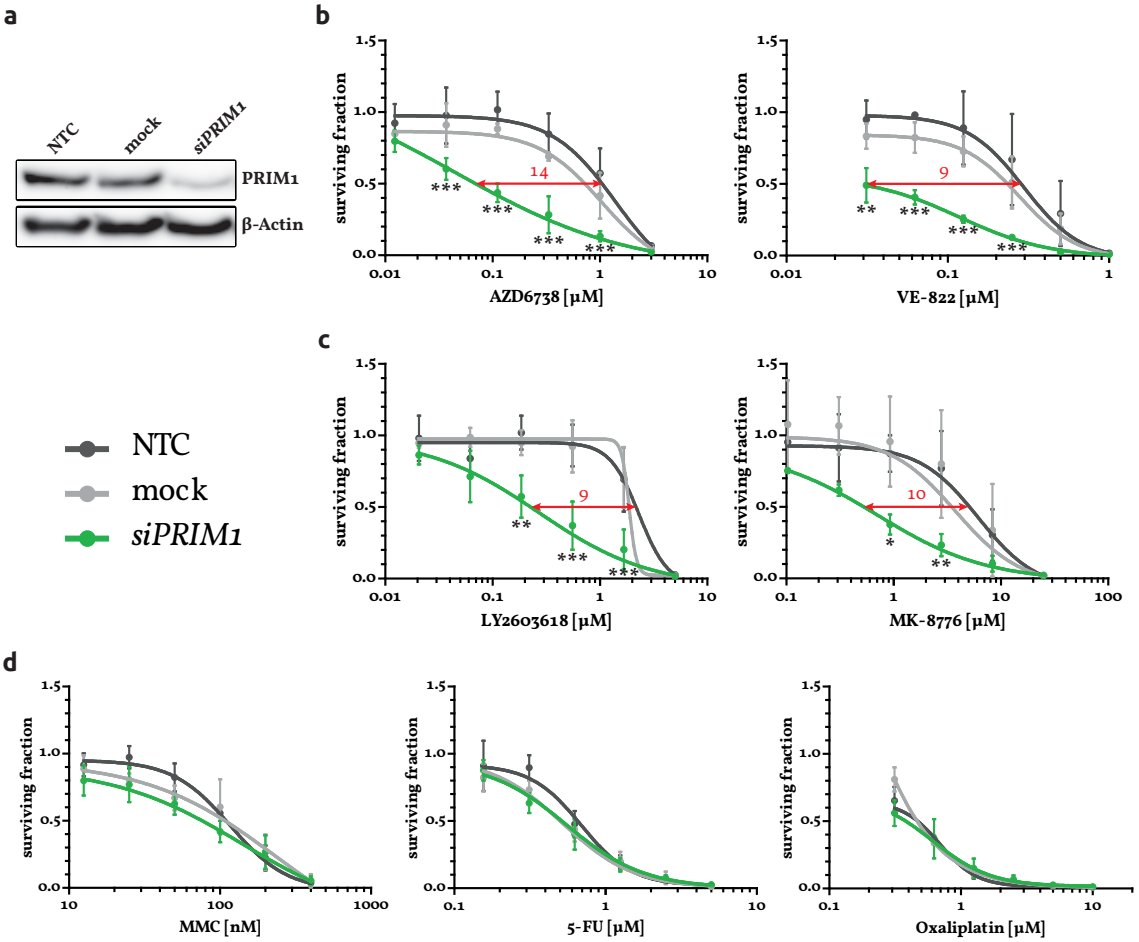

Figure 8 | Sensitization of DLD-1 cells to ATR and CHK1 inhibitors upon *PRIM1* depletion

a | PRIM1 knockdown confirmation via immunoblotting 96 hours after transfection with β-Actin serving as loading control. **b** | Sensitivity assessment of *PRIM1*-depleted cells as compared to NTC and mock-transfected cells via proliferation assay 120 hours after treatment with ATR inhibitors, **c** | CHK1 inhibitors, and **d** | common chemotherapeutics. **Data information** | All data are presented as mean ± SD. Experiments were performed independently (n = 3) with each data point reflecting triplicate wells. Immunoblots were performed independently for each proliferation assay, and representative results are shown. Statistical significance (*$P < 0.05$, **$P < 0.01$, ***$P < 0.001$) refers to *siPRIM1* vs. NTC, and was calculated using a two-way ANOVA with Bonferroni post-test.

4.1.3 Assessing the molecular mechanism of the synthetic lethal relationship between *ATR* and *PRIM1*

After analyzing the detrimental effects of *ATR* and *PRIM1* depletion on different tumor cell lines, we investigated the molecular mechanism underlying this synthetic lethal relationship. Comparison of the cell cycle profiles of $ATR^{+/+}$ and $ATR^{s/s}$ cells expectably revealed a constitutive increase of the G_2/M fraction along with a slight decrease of the S-phase fraction in $ATR^{s/s}$ cells (Figure 10a) due to their loss of DNA damage checkpoint responses [17]. Interestingly, the additional depletion of *PRIM1* induced a significant increase of the S-phase fraction exclusively

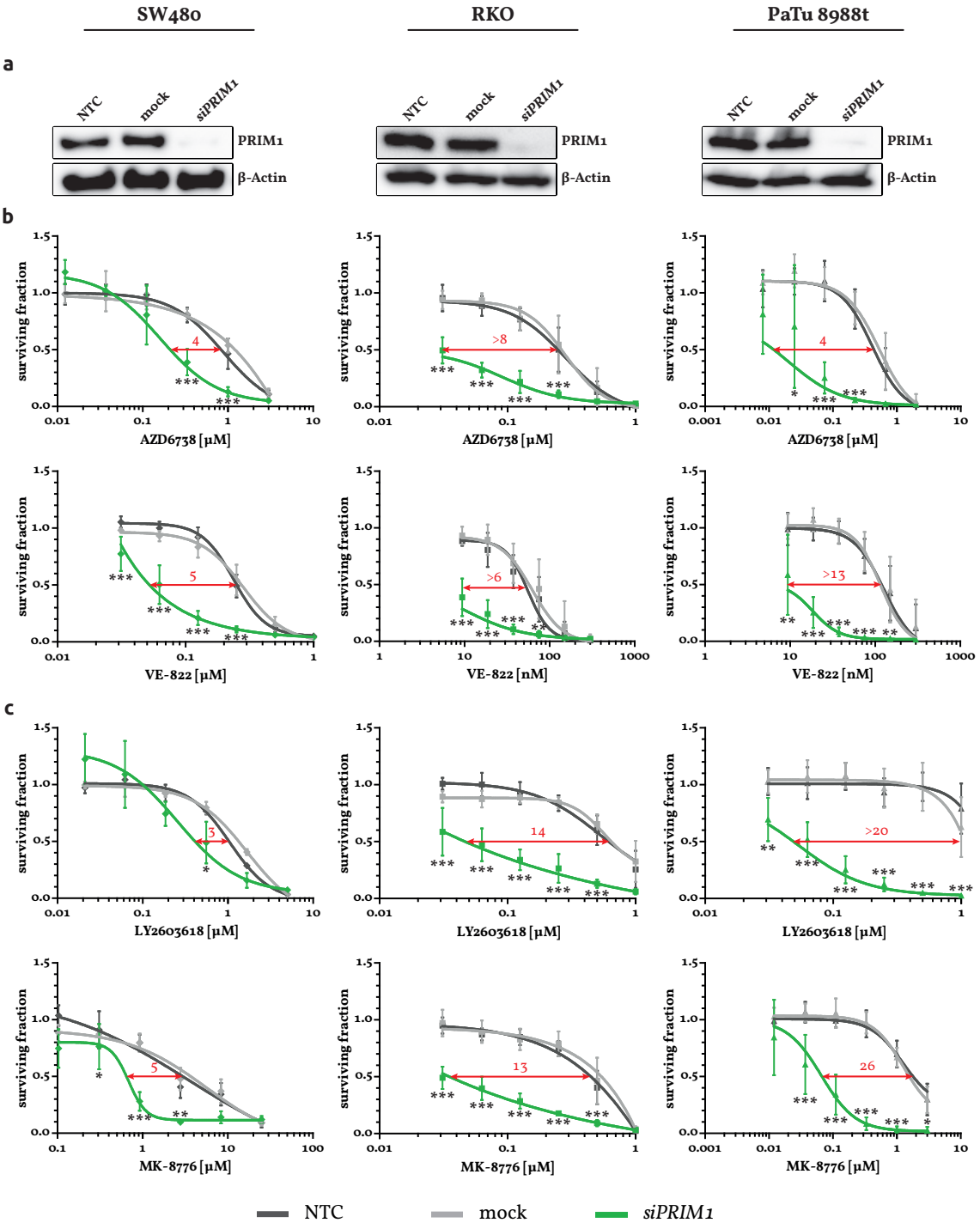

Figure 9 | Sensitization of RKO, SW480, and PaTu 8988t cells to ATR and CHK1 inhibitors upon *PRIM1* depletion

a | PRIM1 knockdown confirmation via immunoblotting 96 hours after transfection with β-Actin serving as loading control. **b** | Sensitivity assessment of *PRIM1*-depleted cells as compared to NTC and mock-transfected cells via proliferation assay 120 hours after treatment with ATR inhibitors and **c** | CHK1 inhibitors. **Data information** | All data are presented as mean ± SD. Experiments were repeated independently (n = 3 for VE-822-, LY2603618-, and MK-8776-treated SW480 cells; n = 4 for AZD6738-treated SW480 cells; n = 5 for all experiments with RKO and PaTu 8988t cells) with each data point reflecting triplicate wells. Immunoblots were performed independently for each proliferation assay, and representative results are shown. Statistical significance (*$P < 0.05$, **$P < 0.01$, ***$P < 0.001$) refers to *siPRIM1* vs. NTC, and was calculated using a two-way ANOVA with Bonferroni post-test.

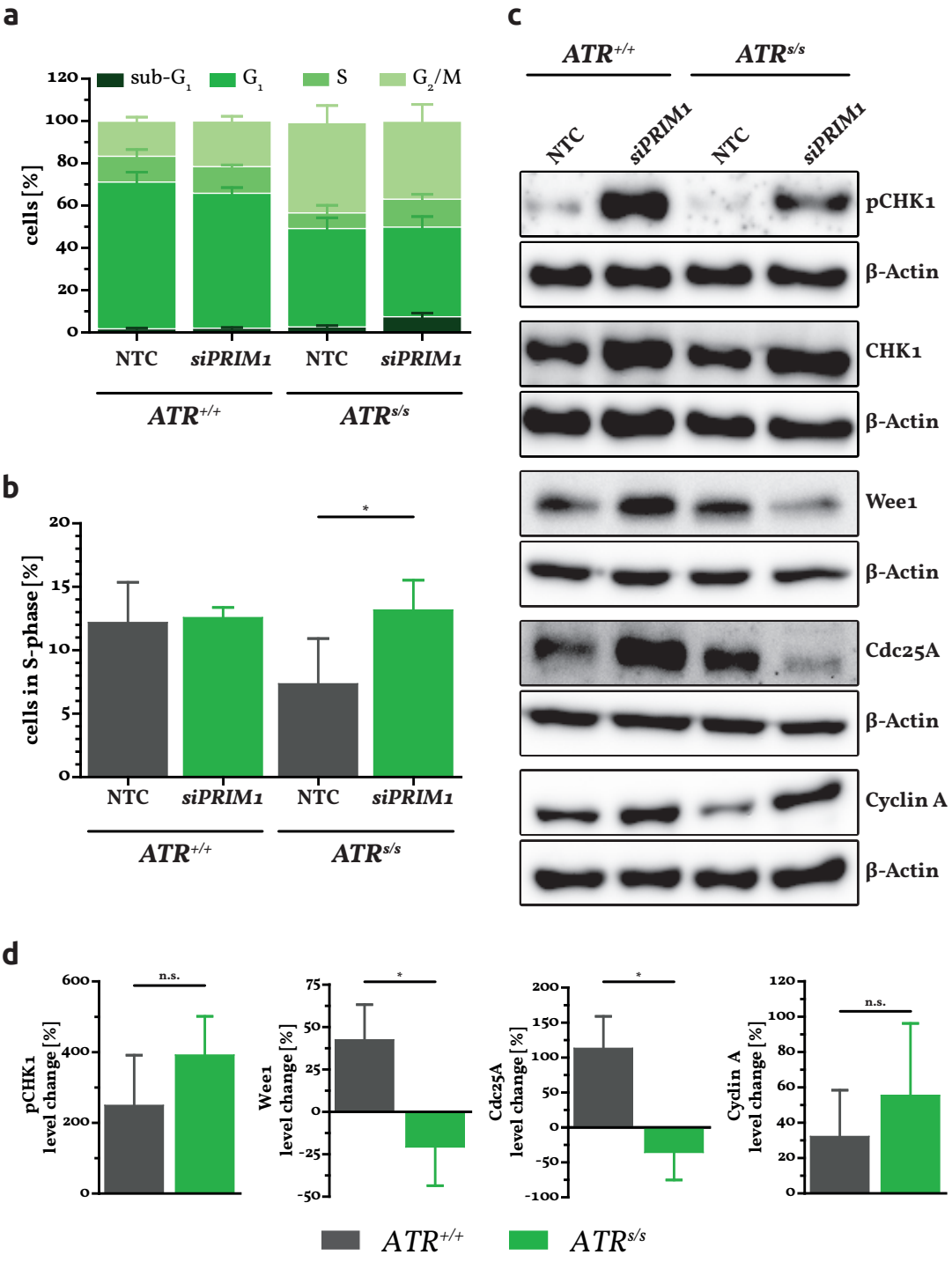

Figure 10 | Impairment of cell cycle progression in *ATR*$^{s/s}$ cells upon *PRIM1* depletion

a | Cell cycle profile assessment of DLD-1 *ATR*$^{+/+}$ and *ATR*$^{s/s}$ cells via FACS analysis 144 hours after *siPRIM1* transfection. **b** | S-phase fraction of the cell cycle profile in detail. **c + d** | Protein quantification in DLD-1 *ATR*$^{+/+}$ and *ATR*$^{s/s}$ cells via immunoblotting 144 hours after *siPRIM1* transfection with β-Actin serving as loading control. Percentage protein change of *PRIM1*-depleted cells was normalized to NTC of DLD-1 *ATR*$^{+/+}$ and *ATR*$^{s/s}$ cells. **Data information** | All data are presented as mean ± SD. Experiments assessing the cell cycle profile were repeated independently (n = 4). Immunoblots were performed independently three times, and representative results are shown. Statistical significance (*$P < 0.05$, n.s. = not significant) was calculated using a two-tailed, unpaired Student's *t* test.

in *ATR*$^{s/s}$ cells (Figure 10b). To identify the responsible mediators of this effect we quantified the cell cycle protein levels of CHK1; Wee1, a key regulator of cell cycle progression [21, 58]; as well as Cdc25A and Cyclin A, mediators of the G_1/S progression (Figure 10c + d). CHK1 protein was activated through phosphorylation upon *PRIM1* depletion. However, this effect appeared to be ATR-independent. The latter is consistent with a previous report of a sufficient CHK1 phosphorylation in *ATR*$^{s/s}$ cells [42]. Furthermore, we observed a *PRIM1*-dependent regulation of the kinase Wee1, i. e. an upregulation in *ATR*$^{+/+}$ and a downregulation in *ATR*$^{s/s}$ cells. Similarly, also the phosphotase Cdc25A was upregulated in *ATR*$^{+/+}$ and downregulated in *ATR*$^{s/s}$

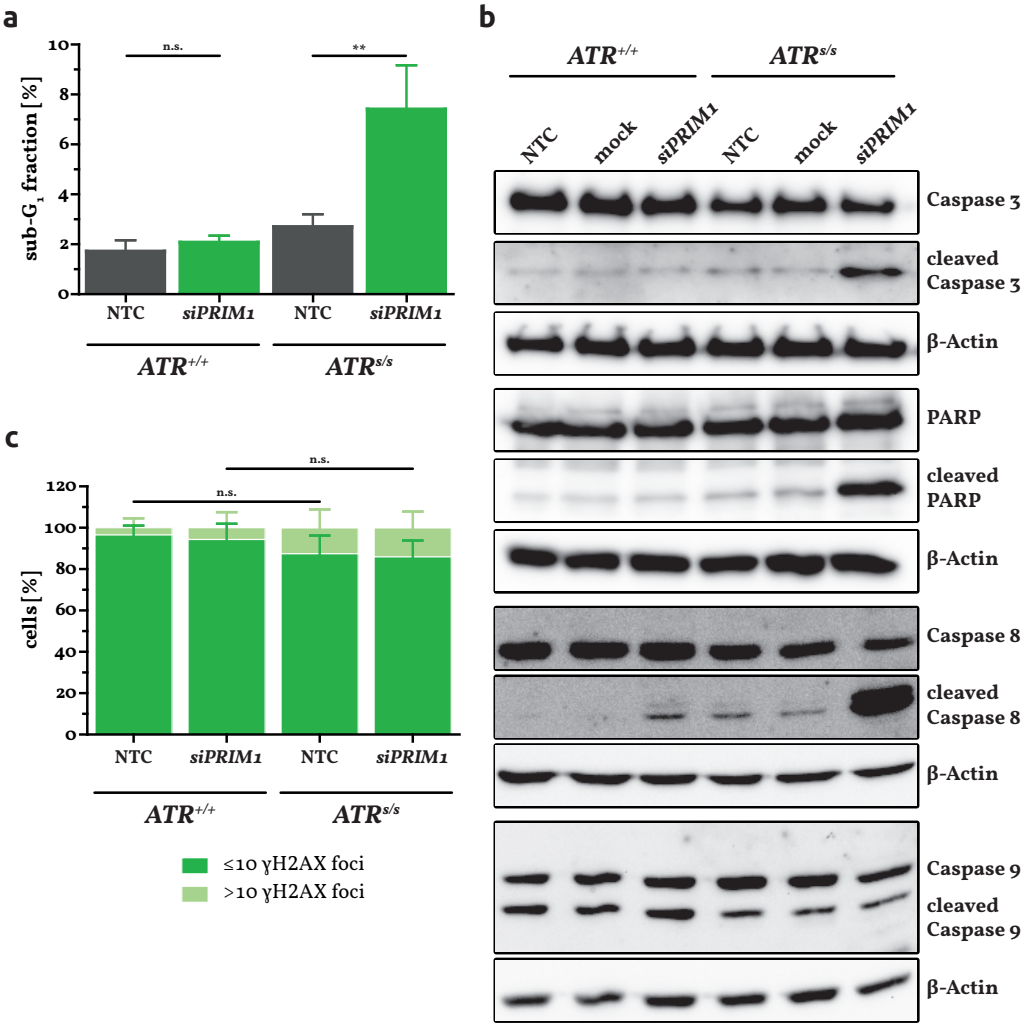

Figure 11 | Induction of apoptosis in *ATR*$^{s/s}$ cells upon *PRIM1* depletion
a | Sub-G_1 fraction of the cell cycle profile (Figure 10a) in detail. **b** | Protein quantification in DLD-1 *ATR*$^{+/+}$ and *ATR*$^{s/s}$ cells via immunoblotting 144 hours after *siPRIM1* transfection with β-Actin serving as loading control. **c** | γH2AX quantification in DLD-1 *ATR*$^{+/+}$ and *ATR*$^{s/s}$ cells via immunocytochemistry 120 hours after *siPRIM1* transfection. **Data information** | All data are presented as mean ± SD. Experiments were repeated independently (n = 4 for the assessed sub-G_1 fraction; n = 3 for the γH2AX foci formation). Immunoblots were performed independently (n = 2 for caspase 3, PARP, and caspase 9; n = 3 for caspase 8), and representative results are shown. Statistical significance was calculated using a two-tailed, unpaired Student's *t* test (**$P < 0.01$, n.s. = not significant).

cells. In contrast, Cyclin A appeared to be slightly upregulated in *ATR*$^{s/s}$ cells upon *PRIM1* depletion as compared to *PRIM1*-depleted *ATR*$^{+/+}$ cells, but this effect did not reach statistical significance.

As the cell cycle profiles also revealed a significant increase of the sub-G_1 fraction in *PRIM1*-depleted *ATR*$^{s/s}$ cells (Figures 10a + 11a) we next investigated the protein levels of the central apoptosis mediators in *ATR*$^{+/+}$ and *ATR*$^{s/s}$ cells upon *PRIM1* depletion (Figure 11b). Consistent with the sub-G_1 data we observed the cleavage of caspase 3, the main effector protease of apoptosis, along with the cleavage of its substrate PARP only in *PRIM1*-depleted *ATR*$^{s/s}$ cells. Similarly, the indicator of extrinsic apoptosis caspase 8 was cleaved *PRIM1*-dependently in *ATR*$^{s/s}$ cells, while caspase 9, an indicator of the intrinsic apoptosis pathway, appeared to be cleaved unspecifically. We additionally investigated the accumulation of DNA damage to test its potential contribution to the observed apoptotic effects by quantifying the formation of γH2AX, a surrogate marker for DNA DSBs [83] (Figure 11c). As *ATR* is a central mediator of DDR, *ATR*-deficient *ATR*$^{s/s}$ cells expectably displayed a slight but not significant increase of γH2AX foci as compared to *ATR*$^{+/+}$ cells with no further augmentation upon *PRIM1* depletion.

In summary, we showed that the detrimental effects of *PRIM1* depletion in *ATR*$^{s/s}$ cells is in part attributable to S-phase impairment with concomitant Wee1 down-regulation and a subsequent activation of the extrinsic apoptotic pathway without evidence of increased DNA damage accumulation.

4.2 Assessing the impact of *POLD1* variants of uncertain significance to treatment with ATR pathway inhibitors

Apart from *PRIM1* also *POLD1*, the catalytic subunit of Polδ, displays synthetic lethal interactions with *ATR*, which has been previously described [41]. This interaction could be of clinical relevance as various *POLD1* variants have been identified in colorectal and other cancers [7, 74, 94]. However, the significance of these variants as potential biomarkers for the targeted treatment of tumors with ATR inhibitors remains enigmatic. Thus, the aim of this second subproject was to establish a *POLD1*-KO model to enable the prediction of the impact of certain variants on the therapeutic response to ATR pathway inhibitors by using various read-outs. Establishing this model, we characterized four *POLD1* variants in regard to their impact on the sensitivity to ATR pathway inhibitors *in vitro* and *in vivo*. Additionally, we assessed their impact on the DNA damage response.

4.2.1 Establishing heterozygous *POLD1*-knockout clones by using CRISPR/Cas9

With recent publications reporting various *POLD1* variants in familial cases of CRC [7, 74, 94], and the identified synthetic lethality of *ATR* and *POLD1* [41] we assessed whether such variants were clinically exploitable for potential treatment with inhibitors targeting the ATR pathway. We therefore used the CRISPR/Cas9 technique to establish a *POLD1*-KO in the CRC cell line DLD-1, which harbors four heterozygous *POLD1* variants [28]. We genotyped multiple single cell colonies and obtained two distinct heterozygous *POLD1*-KO clones (termed g1-2 and g2-1) as well as a $POLD1^{+/+}$ ctrl clone, which was transfected with a scrambled gRNA (Figure 12a). The immunoblot of $POLD1^{+/-}$ g1-2 and g2-1 cells revealed no changes in POLD1 protein expression as compared to $POLD1^{+/+}$ parental and ctrl cells (Figure 12b). To generate a homozygous *POLD1*-KO we first excised the PuroR cassette in g1-2 and g2-1 cell clones mediated by the Cre/loxP recombinase (Figure 12c), and then targeted the second allele. However, despite multiple targeting rounds we were unable to establish a homozygous *POLD1*-KO cell clone.

We confirmed the four heterozygous *POLD1* variants G10V, R506H, R689W, and S746I, which were previously reported in DLD-1 cells [28], in our $POLD1^{+/+}$ parental cells by genome sequencing (Figure 13, upper panel). As the allele specific localization of these variants remained unknown, we used mRNA sequencing to demonstrate that the intact *POLD1* allele of the heterozygous cell clone g1-2 exhibited only the R689W variant, thus being termed $POLD1^{R689W/-}$ (Figure 13, middle

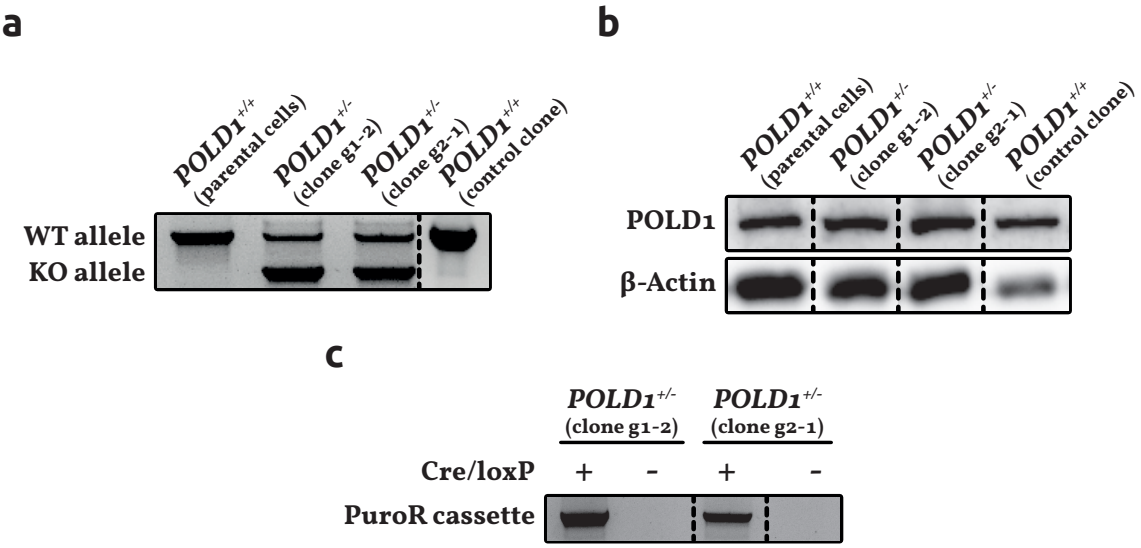

Figure 12 | Generation of a DLD-1 *POLD1*-knockout via CRISPR/Cas9
a | Detection of the *POLD1*-KO and -WT alleles in *POLD1*$^{+/+}$ parental and ctrl cells as well as in *POLD1*$^{+/-}$ g1-2 and g2-1 cells via PCR. **b** | Protein quantification in *POLD1*$^{+/+}$ parental and ctrl cells as well as in *POLD1*$^{+/-}$ g1-2 and g2-1 cells via immunoblotting with β-Actin serving as loading control. **c** | Detection of the Cre/loxP-mediated excision of the PuroR cassette in *POLD1*$^{+/-}$ g1-2 and g2-1 cells via PCR.

panel). The intact *POLD1* allele of the heterozygous cell clone g2-1 exhibited the three other *POLD1* variants G10V, R506H, and S746I (*POLD1*$^{G10V, R506H, S746I/-}$, Figure 13, lower panel). However, according to the data obtained later (no functional significance of POLD1^{G10V}, POLD1^{R506H}, and POLD1^{S746I}), and for convenience we retrospectively termed this cell clone here *POLD1*$^{+/-}$.

4.2.2 Characterizing the functional impact of various *POLD1* variants

After generating heterozygous *POLD1*-KO cell clones, which exclusively expressed either POLD1^{R689W} or POLD1$^{G10V, R506H, S746I}$, we assessed the impact of these variants on POLD1 function. As defects in DNA replication lead to the compensatory activation of DNA repair pathways [38], the functional impairment of POLD1 could be expected to cause compensatory activation of the *ATR* pathway [41]. Thus, we assessed protein and phosphorylation levels of CHK1, the major effector kinase of ATR, in the respective cell clones harboring different *POLD1* VUS. We observed a strong constitutive CHK1 phosphorylation exclusively in *POLD1*$^{R689W/-}$ but not in *POLD1*$^{+/-}$ and *POLD1*$^{+/+}$ cells, an effect which was qualitatively comparable to the effects of siRNA-mediated subtotal *POLD1* depletion (Figure 14a). These data indicated that only POLD1^{R689W} but not POLD1^{G10V}, POLD1^{R506H}, or POLD1^{S746I} had a functional relevance. Therefore, we next assessed the impact of POLD1^{R689W} on DNA replication upon treatment with ionizing radiation (IR) or HU via DNA

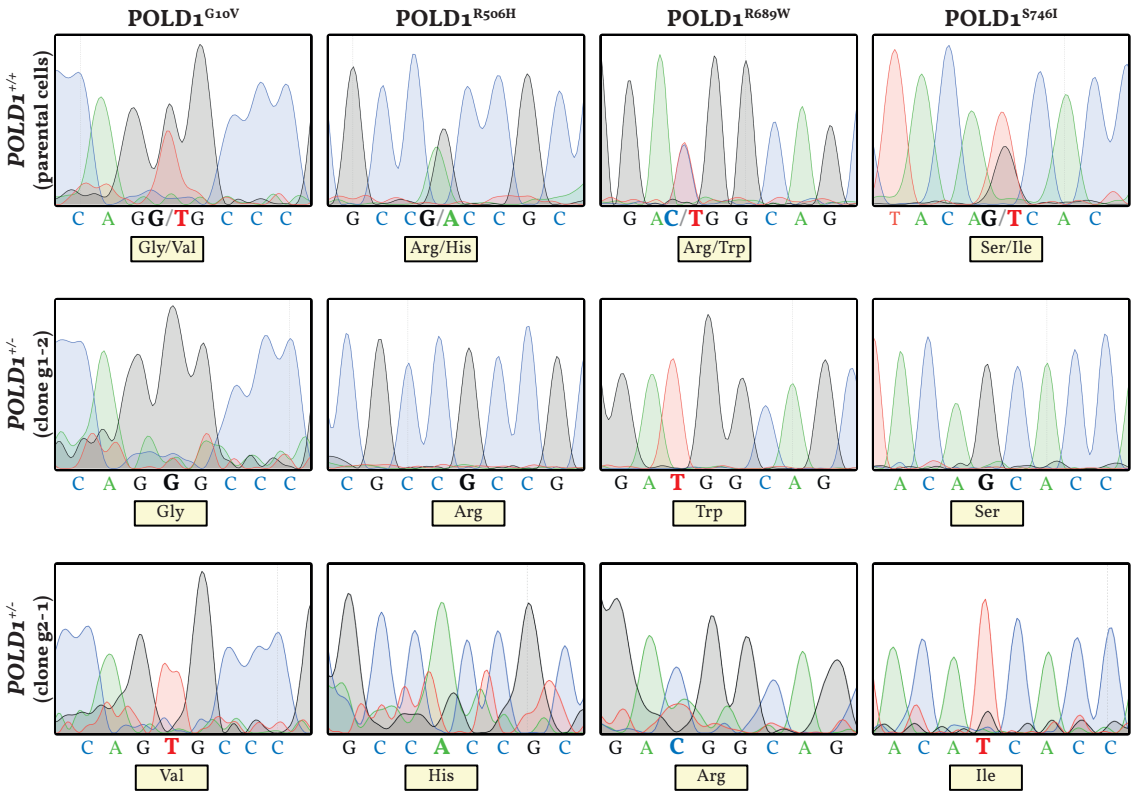

Figure 13 | Allele-specific localization of *POLD1* variants in DLD-1 cells
Localization of *POLD1* variants in *POLD1*$^{+/+}$ parental cells as well as the *POLD1*$^{+/-}$ g1-2 and g2-1 cell clones via genome and mRNA sequencing.

fiber assays (Figure 20). We assessed the elongation rate, which correlates with the replication pace; 2nd pulse origins, which represent new replication origin firing of dormant origins; and stalled replication forks as marker for the physiological response to replication stress. The constitutive overall elongation rate was slightly higher in *POLD1*$^{R689W/-}$ than in *POLD1*$^{+/+}$ cells. Upon IR treatment, however, the elongation rate decreased only in *POLD1*$^{R689W/-}$ cells, but remained unchanged in *POLD1*$^{+/+}$ cells (Figure 14b). Furthermore, we observed that HU treatment induced a stronger decrease of 2nd pulse origins in *POLD1*$^{+/+}$ than in *POLD1*$^{R689W/-}$ cells (Figure 14c). Consistently, stalled replication forks were only increased in *POLD1*$^{+/+}$ but not in *POLD1*$^{R689W/-}$ cells upon HU treatment (Figure 14d).

In summary, our data indicated that of the four previously described *POLD1* variants in DLD-1 cells only POLD1^{R689W} had an impact on gene function, as compensatory ATR pathway activation and impairment of DNA replication, respectively, were exclusively observable in *POLD1*$^{R689W/-}$ cells.

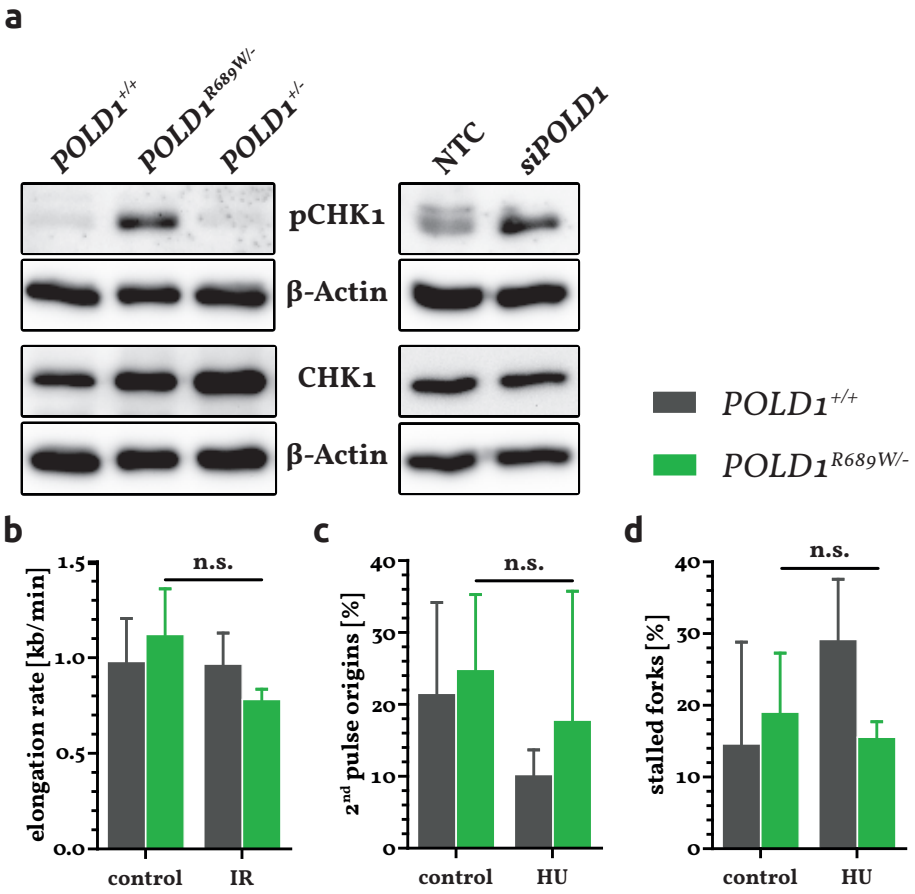

Figure 14 | Functional characterization of POLD1^{R689W} in DLD-1 cells
a | Protein quantification in *POLD1*$^{+/+}$, *POLD1*$^{R689W/-}$, and *POLD1*$^{+/-}$ cells via immunoblotting in a constitutive state as well as 120 hours after *siPOLD1* transfection with β-Actin serving as loading control. **b** | Quantification of the elongation rate, **c** | 2nd pulse origins, and **d** | stalled replication forks in *POLD1*$^{+/+}$ and *POLD1*$^{R689W/-}$ cells via DNA fiber assay upon IR or HU treatment. **Data information** | All data are presented as mean ± SD. Experiments were performed independently (n = 3) with at least 100 DNA fibers analyzed in each experiment. Immunoblots were performed independently (n = 3), and representative results are shown. Statistical significance was calculated using a two-tailed, unpaired Student's *t* test (n.s. = not significant).

4.2.3 Assessing the impact of POLD1^{R689W} on the sensitivity of DLD-1 cells to ATR pathway inhibitors *in vitro*

We first assessed the impact of POLD1^{R689W} on the cellular sensitivity to ATR and CHK1 inhibitors *in vitro*. Compared to *POLD1*$^{+/+}$ parental and ctrl cells, we observed only in *POLD1*$^{R689W/-}$ but not in *POLD1*$^{+/-}$ cells an increased sensitivity to the selective ATR inhibitors AZD6738 and VE-822 [47, 78] with IC_{50} ratios of 11 and 6, respectively (Figure 15a). Similarly, only *POLD1*$^{R689W/-}$ but not *POLD1*$^{+/-}$ cells displayed an increased sensitivity to the selective CHK1 inhibitors LY2603618 and MK-8776 [19, 89, 99] with IC_{50} ratios of 5 and 4, respectively (Figure 15b). To exclude a general and unspecific drug hyper-sensitivity mediated by POLD1^{R689W} we treated cells with common chemotherapeutics including MMC, 5-FU, carboplatin,

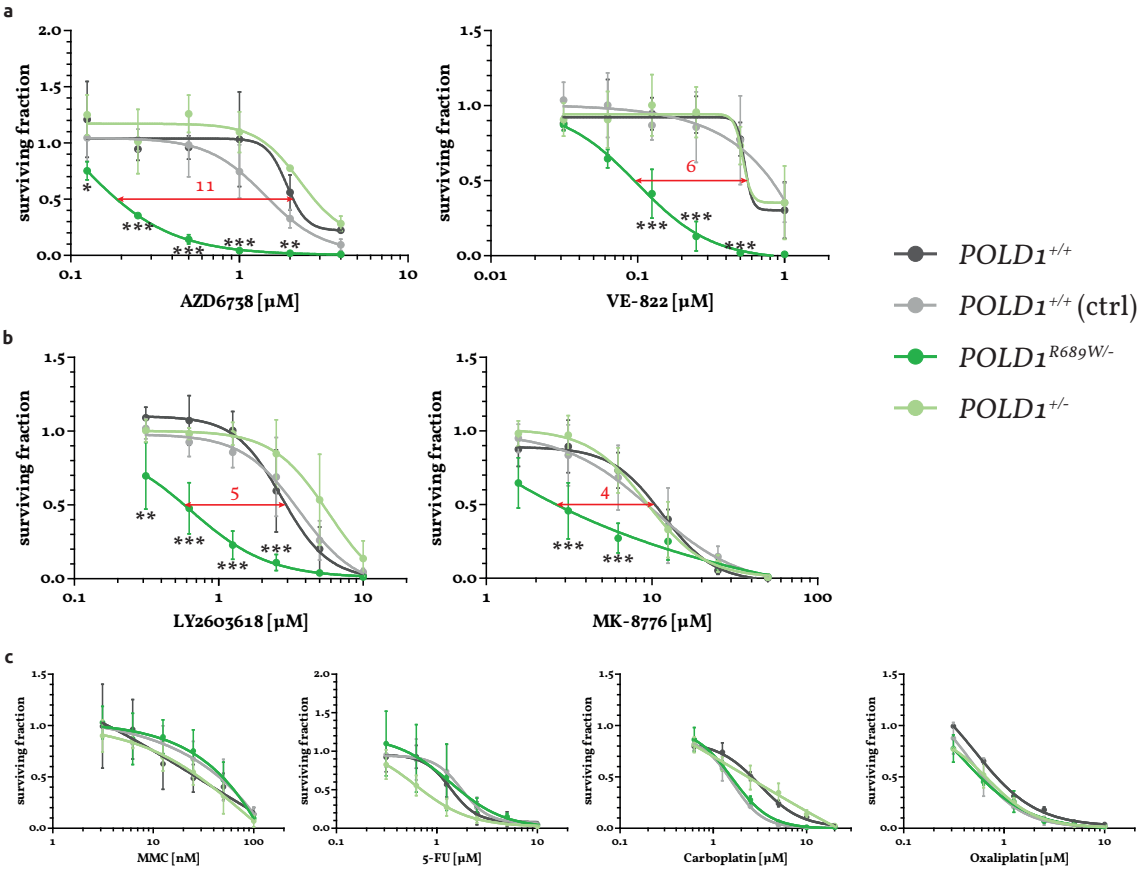

Figure 15 | Sensitization of DLD-1 cells to ATR and CHK1 inhibitors *in vitro* mediated by POLD1^{R689W}

Sensitivity assessment of *POLD1*$^{R689W/-}$ cells as compared to *POLD1*$^{+/-}$ and *POLD1*$^{+/+}$ parental and ctrl cells 120 hours after treatment with **a** | ATR inhibitors, **b** | CHK1 inhibitors, and **c** | common chemotherapeutics. **Data information** | All data are presented as mean ± SD. Experiments were repeated independently (n = 3 for the treatment with ATR inhibitors, MMC, and carboplatin; n = 4 for the treatment with CHK1 inhibitors, 5-FU, and oxaliplatin) with each data point reflecting triplicate wells. Statistical significance (*P < 0.05, **P < 0.01, ***P < 0.001) refers to *siPRIM1* vs. NTC, and was calculated using a two-way ANOVA with Bonferroni post-test.

and oxaliplatin, and observed no POLD1^{R689W}-dependent differences in proliferation (Figure 15c).

In summary, our *in vitro* data showed that only the POLD1 variant R689W but not G10V, R506H, or S746I sensitized DLD-1 cells specifically to inhibitors targeting ATR or CHK1, and that this proliferation inhibitory effect is not caused by a general and unspecific drug hyper-sensitivity mediated by POLD1^{R689W}.

4.2.4 Assessing the impact of POLD1^{R689W} on the sensitivity of DLD-1 cells to the ATR inhibitor AZD6738 *in vivo*

We next extended our *in vitro* data by using a murine xenograft tumor model to assess the sensitivity of *POLD1*$^{+/+}$ and *POLD1*$^{R689W/-}$ cells to the ATR inhibitor AZD6738 *in vivo*. Treatment of mice with vehicle or AZD6738 [50 mg/kg] was well tolerated, as

loss of body weight in the beginning of this experiment did not exceed 10 %, and later even normalized to the initial body weight, thus remaining in the animal welfare guidelines (Figure 16a). Regarding tumor size, we observed the strongest growth in vehicle-treated *POLD1*$^{+/+}$ tumors (Figure 16b) nearly quadrupling their original size (Figure 16c). While the R689W-mediated impairment of POLD1 alone or the ATR-inhibition by AZD6738 alone only slightly decreased tumor size and growth, the combined impairment of POLD1 and inhibition of ATR strongly decelerated

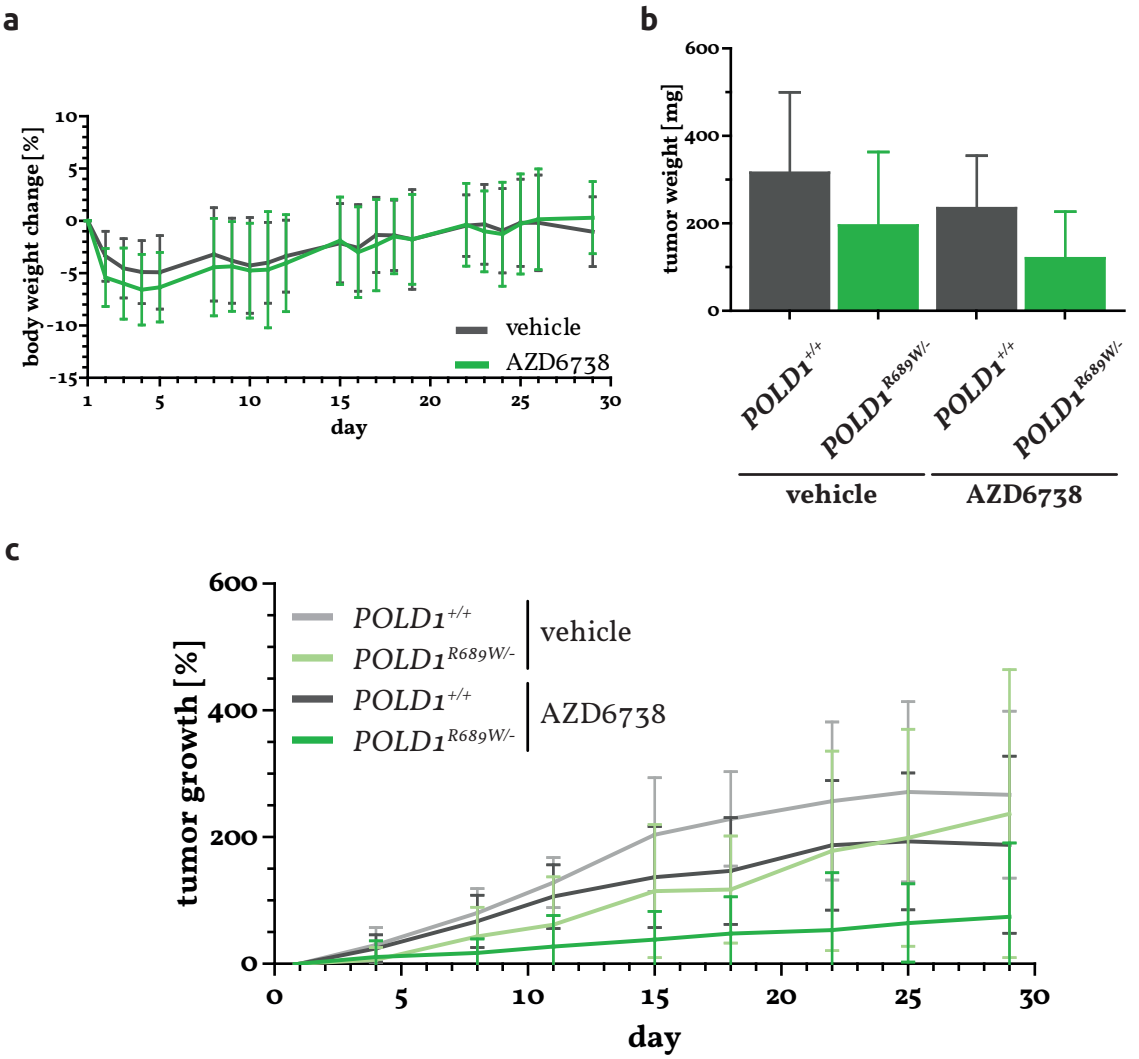

Figure 16 | Sensitization of DLD-1 cells to the ATR inhibitor AZD6738 *in vivo* mediated by POLD1^{R689W}

a | Body weight change assessment of vehicle- or AZD6738-treated mice during the four-week treatment. **b** | Weight assessment of *POLD1*$^{+/+}$ or *POLD1*$^{R689W/-}$ tumors four weeks after constant treatment with vehicle or AZD6738. **c** | Growth assessment of *POLD1*$^{+/+}$ or *POLD1*$^{R689W/-}$ tumors during the four-week treatment with vehicle or AZD6738. **Data information** | All data are presented as mean ± SD with six mice in the vehicle-treated *POLD1*$^{+/+}$ tumor group, six mice in the AZD6738-treated *POLD1*$^{+/+}$ tumor group, five mice in the vehicle-treated *POLD1*$^{R689W/-}$ tumor group, and four mice in the AZD6738-treated *POLD1*$^{R689W/-}$ tumor group.

tumor growth as illustrated by AZD6738-treated *POLD1*$^{R689W/-}$ tumors not even doubling their original size during the entire observation period (Figure 16b + c).

In summary, these data showed that the POLD1^{R689W} variant sensitized DLD-1 cells specifically to the ATR inhibitor AZD6738 also *in vivo*. Together with the *in vitro* data these observations are therefore consistent with our functional data regarding CHK1 phosphorylation and impaired DNA replication. However, the *in vivo* data are limited by the fact, that we could only analyze four mice in the important group of AZD6738-treated *POLD1*$^{R689W/-}$ tumors, due to the unexpected low tumor take rate. The *in vivo* data presented here are thus preliminary, representing distinct trends, but without a statistical significance yet. Hence, further verification in additional xenograft *in vivo* experiments is mandatory.

5 Discussion

5.1 Inactivation of PRIM1 function sensitizes cancer cells to ATR and CHK1 inhibitors

As the principle of synthetic lethality offers new approaches for an individualized and targeted cancer therapy with reduced side effects [46, 70], we here verified and characterized the previously identified synthetic lethal relationship between the DNA damage sensing protein ATR and the catalytic subunit of primase of the Polα-primase complex PRIM1 [41].

5.1.1 Verifying the synthetic lethality

Initially, we used *ATR*$^{s/s}$ cells of the human CRC cell line DLD-1, which were genetically engineered to homozygously harbor the *ATR* "Seckel" variant A2101G [73], resulting in a subtotal ATR protein depletion with increased sensitivity to DNA ICL agents but no significant effect on cell growth or viability [30, 31, 42, 101]. As this subtotal ATR protein depletion mimicked the incomplete pharmacological inhibition of ATR more closely than a complete and lethal *ATR*-KO [17], this model proved to be ideally suited for our experiments. Additionally, we established an *ATR* re-expressing rescue cell clone to exclude clonal variation as a confounding artifact. By demonstrating the proliferation inhibition of *ATR*$^{s/s}$ cells upon siRNA-mediated *PRIM1* depletion, an effect which was partly reversible upon *ATR* re-expression, we confirmed the synthetic lethal relationship between *ATR* and *PRIM1*. To exclude potential off-target effects of *siPRIM1* it would be necessary to treat *ATR*$^{s/s}$ cells with a *PRIM1* inhibitor. However, selective PRIM1 inhibitors remain to be developed. To

overcome this problem nonetheless, we treated *ATR*$^{s/s}$ cells with ST1926, a chemical inhibitor of Polα of the Polα-primase complex [1, 33, 37]. As Polα functionally depends on the preceding RNA primer synthesis by primase [49, 77, 97], a functional hierarchy of the Polα-primase complex may be deduced with primase being epistatic to Polα. Thus, we assumed that targeting downstream components might cause similar effects as targeting primase. Indeed, we observed similar proliferation inhibition of *ATR*$^{s/s}$ cells upon treatment with ST1926, thus indicating off-target effects of *siPRIM1* to be unlikely. Additionally, these data demonstrated due to the functional hierarchy of the Polα-primase complex that not only primase, i. e. its catalytic subunit *PRIM1*, but also the functional downstream Polα, i. e. its catalytic subunit *POLA1*, could potentially represent a novel target for therapeutic approaches using ATR inhibitors.

5.1.2 *In vitro* validation

As the chemical inhibition of ATR is known to eliminate certain subsets of cancer cells, which is partly attributable to synthetic lethality, we next assessed whether the proliferation inhibitory effects on *PRIM1*-depleted cells with a genetically induced *ATR* deficiency were also elicitable in *PRIM1*-depleted, *ATR*-proficient cells with a chemically induced ATR deficiency. We therefore used clinically relevant inhibitors targeting ATR [47, 78] and its main effector kinase CHK1 [19, 89, 99]. In fact, both ATR and CHK1 inhibitors decreased proliferation of DLD-1 cells upon *PRIM1* depletion. Importantly, we were able to generalize our data by demonstrating similar results in two additonal CRC cell lines, SW480 and RKO, as well as in the pancreatic cancer cell line PaTu 8988t. As these cell lines exhibit both microsatellite stability and instability, respectively, we showed that our data are independent of the microsatellite instability status. Therefore, inactivated *PRIM1* in cancers could represent a predictive biomarker for their sensitivity to ATR and CHK1 inhibitors.

5.1.3 Mechanistic insights

Mechanistically, we demonstrated an increased S-phase fraction in *ATR*$^{s/s}$ cells upon *PRIM1* depletion and a concomitant upregulation of phosphorylated CHK1 and downregulation of Cdc25A, thus indicating cell cycle arrest during S-phase [63, 76]. However, the virtually undiminished protein levels of Cyclin A in *PRIM1*-depleted *ATR*$^{s/s}$ cells rather suggested an S-phase stasis than a classical S-phase arrest [9]. This assumption is consistent with Hurley and colleagues, describing that ionizing radiation of *ATR*$^{s/s}$ cells led to a prolonged S-phase which closely resembled S-phase stasis [42]. The induced S-phase stasis in cells simultaneously depleted of both *ATR* and *PRIM1* might thus represent an unresolvable replication catastrophe.

Besides cell cycle impairment and perhaps even more importantly, apoptosis contributed to the *PRIM1*-dependent proliferation inhibitory effects, as demonstrated by the increased sub-G_1 fraction and the cleavage of the common apoptosis effector enzymes caspase 3 and PARP exclusively in *PRIM1*-depleted $ATR^{s/s}$ cells. Additionally, the simultaneous *ATR*- and *PRIM1*-dependent cleavage of caspase 8 but not of caspase 9 hinted at an extrinsic rather than an intrinsic apoptosis induction [13]. Typically, extrinsic apoptosis is predominantly mediated by death receptors [13]. Additionally, downregulation of Wee1, as observed in our experiments in $ATR^{s/s}$ cells upon *PRIM1*-depletion, also leads to apoptosis through increased surface expression of death receptors [34, 91]. As the accumulation of DNA damage might also contribute to apoptosis, we furthermore quantified γH2AX foci formation, which serves as surrogate marker for DNA damage in terms of DSBs [83]. Interestingly, we did not observe an increase of DSBs, and thus excluded their contribution to apoptosis. Therefore, apoptosis induced by the downregulation of Wee1 might represent a protective cellular response to the precedingly induced replication catastrophe in *ATR*-deficient cells upon *PRIM1*-depletion.

5.1.4 Role of *PRIM1* in cancer

Little is known about the prevalence of genetic alterations of *PRIM1* in cancer. The amplification of a large region including the *PRIM1* gene locus was reported in osteosarcoma [104], and upregulation of *PRIM1* gene expression was reported in cancers of lung [102] and breast [54]. Besides these few reports about altered gene expression, only 0.2 % of around 35 000 tested tumor samples showed variants in *PRIM1* according to the Catalogue Of Somatic Mutations In Cancer (COSMIC). For comparison, the COSMIC database lists around 150 000 and more than 240 000 tested tumor samples for the intensively characterized tumor suppressor gene *TP53* and the proto-oncogene *KRAS*, respectively [87]. This insufficiency of data regarding *PRIM1* alterations in cancer illustrates the need to further characterize the role of *PRIM1* in cancer, as its potential as novel target for future therapeutic approaches in defined small subsets of tumors still remains poorly defined.

5.1.5 Future studies

The synthetic lethal relationship between *ATR* and *PRIM1* was recently identified and in this dissertation for the first time characterized. To validate the clinical significance of this relationship future studies are mandatory. In our experiments we used siRNA to deplete *PRIM1*. Due to the lack of selective PRIM1 inhibitors we were not able to directly exclude off-target effects of *siPRIM1*, which should be further evaluated when suitable chemical compounds are developed. Instead, we indirectly

excluded off-target effects by using ST1926, a selective Polα inhibitor [1, 33, 37]. Besides ST1926, other chemical compounds were reported to selectively inhibit Polα including dehydroaltenusin [56, 62], demethoxydehydroaltenusin [51], and depeptide alcohols [50]. As the efficacy of these inhibitors on the proliferation of $ATR^{s/s}$ cells is unknown, this should be further investigated, especially with a potential clinical application in mind. Furthermore, the ST1926-mediated proliferation inhibition of $ATR^{s/s}$ cells indicated that the inhibition of any compound of the Polα-primase complex together with impairment of *ATR* could induce synthetic lethality. Thus, the potential synthetic lethal relationship between *ATR* and *POLA1*, the catalytic subunit of Polα, should be verified using *siPOLA1* and further characterized similar to *PRIM1*, as these data could facilitate a novel concept for *ATR*-deficient tumors being treated with inhibitors targeting the Polα-primase complex. This future characterization and the here demonstrated *in vitro* characterization of the synthetic lethality between *ATR* and *PRIM1* could then also be extended to the *in vivo* setting, e. g. a murine xenograft tumor model as proof of principle prior to clinical trials. Beside the above mentioned identification of *PRIM1* variants in tumors, also *POLA1* variants (0.9 % of around 35 000 tested samples) and *ATR* variants (2.3 % of around 51 000 tested samples) were identified in tumors [87]. With regard to the later discussed impact of the $POLD1^{R689W}$ variant on the cellular sensitivity to ATR pathway inhibitors, the systematical evaluation of prevalence as well as the identification and characterization of gene variants of the Polα-primase complex and also *ATR* should be the aim of future studies.

5.2 Sensitization of DLD-1 cancer cells to ATR pathway inhibitors through the POLD1^{R689W} variant

By screening an siRNA library we previously identified *ATR* to act synthetically lethal not only with *PRIM1*, but also with *POLD1*, the catalytic subunit of Polδ [41]. While VUS in *POLD1* have been recently identified in colorectal and other cancers [7, 74, 94], their significance as potential biomarkers for a targeted therapy with inhibitors of the ATR pathway remained unknown. Yet, the identification and characterization of VUS is of importance as illustrated by the example of *BRCA1/2*. Patients with identified pathogenic *BRCA1/2* variants are recommended for consideration of prophylactic surgeries due to their *BRCA1/2* VUS-mediated higher risk of tumorigenesis [100]. Thus, we here established a cellular *POLD1*-KO model system to determine the pathogenicity of individual *POLD1* VUS.

5.2.1 *POLD1*-knockout

The CRC cell line DLD-1 harbors the four heterozygous POLD1 variants G10V, R506H, R689W, and S746I [28] with unknown allele localization. To establish a *POLD1*-KO model system and to identify the variant's allele specific localization we applied the CRISPR/Cas9 technique in order to separately disrupt each *POLD1* allele. Following genome/mRNA sequencing, we demonstrated that G10V, R506H, and S746I are localized together on one *POLD1* allele, while R689W is isolated on the second *POLD1* allele. The obtained heterozygous KO clones therefore exclusively expressed either POLD1$^{G10V,\ R506H,\ S746I}$ (termed *POLD1*$^{+/-}$) or POLD1^{R689W} (termed *POLD1*$^{R689W/-}$), respectively. By generating KO cell clones with this exclusive expression of certain variants we achieved an ideal model system for the functional characterization of *POLD1* VUS. Despite multiple targeting rounds, we were not able to establish a homozygous *POLD1*$^{-/-}$ clone, indicating *POLD1* to be an essential gene in cancer cells. This hypothesis is further supported by a study by Uchimura *et al.* [92], demonstrating in a murine KO model that *POLD1* is also essential for embryonic development.

5.2.2 Mechanistic insights

In our system, only POLD1^{R689W} but not POLD1$^{G10V,\ R506H,\ S746I}$ had an impact on gene function as shown by the compensatory activation of the ATR pathway and the concomitantly strong increase of CHK1 phosphorylation exclusively in *POLD1*$^{R689W/-}$ cells. Because CHK1 is activated in response to DNA damage [76], our data indicated that the POLD1^{R689W} variant might increase endogenous DNA damage. Con-

sistent with this hypothesis, its *Saccharomyces cerevisiae* analog POLD1^{R696W} was reported to cause a catastrophic genomic instability and a mutator phenotype in yeast [18, 60, 61]. With the data regarding the POLD1^{R689W}-mediated increased sensitivity to ATR pathway inhibitors in mind, the assessment of CHK1 phosphorylation could therefore provide a useful biomarker to identify *POLD1*-VUS which induce an increased sensitivity to ATR inhibitors in a clinical setting [53].

To mechanistically assess the impact of POLD1^{R689W} during DNA replication more accurately we also applied DNA fiber assays. The observed constitutive increase of elongation rate in *POLD1*$^{R689W/-}$ cells could be attributable to a reduction of nucleotide selectivity caused by the POLD1^{R689W} variant [60, 61]. In contrast, IR-treatment led to a decreased elongation rate in *POLD1*$^{R689W/-}$ cells as compared to *POLD1*$^{+/+}$ cells. This could be explained by DNA damage overload caused by additional induction of extrinsic DNA damage in cells that already harbor a mutator phenotype mediated by POLD1^{R689W}, ultimately leading to irreversible instability of DNA fibers. Of note, the R689W variant is located in the polymerase active domain of POLD1, while no variant within the exonuclease domain was identified in *POLD1*$^{R689W/-}$ cells. Thus, the proofreading function can be expected to be intact, as has been previously shown for POLD1^{R696W}, the yeast analog of POLD1^{R689W} [18]. However, elevated levels of nucleotides, as caused by the POLD1^{R689W} variant [60], result in a switch from exonuclease to polymerase activity [32]. In combination with the nucleotide selectivity defects mediated by POLD1^{R689W} [60, 61] this could explain the mutator phenotype despite an intact proofreading exonuclease domain. Unexpectedly, POLD1^{R689W} did not have an impact on the ongoing replication process, even upon treatment with HU, which inhibits the ribonucleotide reductase [103], resulting in decreased levels of nucleotides, and thus a blocked replication process. This could be explained by the already mentioned POLD1^{R689W}-induced increase of nucleotide levels [60], consecutively antagonizing the effects of HU.

5.2.3 *In vitro* and *in vivo* validation

We next assessed the impact of POLD1^{R689W} on the cellular sensitivity to ATR pathway inhibiting chemical agents *in vitro*, using clinically relevant inhibitors of ATR [47, 78] and CHK1 [19, 89, 99]. In fact, both ATR and CHK1 inhibitors decreased proliferation specifically of *POLD1*$^{R689W/-}$ but not *POLD1*$^{+/-}$ cells. Importantly, no significant proliferation differences were observable between these cells upon treatment with common chemotherapeutics, excluding a general and unspecific drug hypersensitivity mediated by POLD1^{R689W}. As a proof of principle prior to clinical trials, we further tested the effects of the ATR inhibitor AZD6738 on *POLD1*$^{R689W/-}$ cells in a murine xenograft tumor model *in vivo*. Only the simultaneous impairment of both POLD1 and ATR (AZD6738-treated *POLD1*$^{R689W/-}$ tumors) caused a trend of

decelerated tumor growth, while the impairment of either POLD1 alone (vehicle-treated *POLD1*$^{R689W/-}$ tumors) or ATR alone (AZD6738-treated *POLD1*$^{+/+}$ tumors) had no discernible effects on tumor growth as compared to vehicle-treated *POLD1*$^{+/+}$ tumors.

5.2.4 Comparison with theoretical prediction tools

We compared our data defining the functional significance of the investigated *POLD1* variants with data from various pathogenicity prediction tools, including PON-P2, a machine learning-based classifier, which groups variants into pathogenic, neutral, or unknown classes, based on random forest probability score [71, 79]; PolyPhen-2, calculating the naive Bayes posterior probability of a variant's impact on protein function to be possibly/probably damaging or benign (non-damaging) [2, 20]; PROVEAN, which uses an alignment-based score to discriminate between deleterious and neutral effects on protein function [14, 43]; and MutationAssessor, calculating a functional impact score by using evolutionary conservation patterns [16, 81]. According to these prediction tools, POLD1^{G10V} and POLD1^{S746I} variants have no or only low functional impact (Table 9), which is in concordance with our data on these variants. In contrast, POLD1^{R506H} and POLD1^{R689W} are both predicted by PON-P2 and PROVEAN to be pathogenic, while they are differently classified by PolyPhen-2 and MutationAssessor regarding their damaging potential and functional impact score, respectively, with POLD1^{R689W} achieving a stronger functional impairment. However, despite the predicted functional significance and pathogenicity of POLD1^{R506H}, we demonstrated that in our model only POLD1^{R689W} had a functional impact on CHK1 phosphorylation, DNA replication, and cellular sensitivity to inhibitors of the ATR pathway. Several explanations for these partly inconsistent data might be possible, including an inaccuracy and thus false classification by the applied prediction tools. Furthermore, the fact that we did not analyze the POLD1^{R506H} variant alone, but only in combination with the variants POLD1^{G10V} and POLD1^{S746I}, which could cause antagonizing or protective effects, could also be an explanation. The existence of such potential "revertant" variants has already been described for *BRCA2* in a similar clinical context [6, 25]. Taken together, algorithm-based, theoretical prediction tools to preliminarily identify pathogenic variants might yield the most accurate estimation of pathogenicity only when combined with practical functional KO model systems, thus facilitating clinical-therapeutic approaches for specific VUS.

Table 9 | Pathogenicity for *POLD1* variants according to different prediction tools with investigated variants being highlighted

Variant	Citation	Prediction tool			
		PON-P2	PolyPhen-2	PROVEAN	Mutation Assessor
p.G10V c.29G>T	[28]	unknown (0.398)	benign (0.041)	neutral (-1.407)	neutral (0.55)
p.V295M c.883G>A	[7]	unknown (0.703)	benign (0.410)	neutral (0.412)	neutral (0.09)
p.D316H c.946G>C	[7]	pathogenic (0.941)	probably damaging (1.000)	deleterious (-6.857)	high (3.69)
p.D316G c.947A>G	[7]	pathogenic (0.919)	probably damaging (1.000)	deleterious (-6.857)	high (3.69)
p.P327L c.981C>G	[74]	pathogenic (0.947)	probably damaging (0.999)	deleterious (-9.824)	high (3.74)
p.S370R c.1110C>G	[74]	unknown (0.560)	benign (0.407)	deleterious (-4.259)	medium (3.115)
p.R409W c.1225C>T	[7]	pathogenic (0.963)	probably damaging (1.000)	deleterious (-7.859)	high (3.74)
p.G426S c.1276G>A	[74]	unknown (0.237)	benign (0.042)	neutral (-0.579)	neutral (-0.485)
p.L474P c.1421T>C	[7, 94]	pathogenic (0.937)	probably damaging (1.000)	deleterious (-6.735)	high (3.74)
p.S478N c.1433G>A	[7, 74, 94]	pathogenic (0.759)	probably damaging (0.998)	deleterious (-2.820)	high (4.215)
p.R506H c.1517G>A	[28]	pathogenic (0.955)	possibly damaging (0.755)	deleterious (-4.922)	medium (2.86)
p.R521Q c.1562G>A	[7]	pathogenic (0.957)	possibly damaging (0.816)	deleterious (-3.464)	medium (3.255)
p.R689W c.2065C>T	[28]	pathogenic (0.973)	probably damaging (0.987)	deleterious (-7.978)	high (4.56)
p.S746I c.2237G>T	[28]	unknown (0.475)	benign (0.143)	deleterious (-3.178)	medium (2.92)

5.2.5 Clinical implications

Regarding a clinical-translational perspective, multiple heterozygous germline variants in *POLD1* have been identified in various cancer types, including colon, endometrium, breast, or brain tumors [7, 74, 94]. Thus, *POLD1* could represent a tumor susceptibility gene. Most of the variants that are predicted to be functionally significant (Table 9) are located in the proofreading exonuclease domain of POLD1, presumably impairing the repair capacity of Polδ, and thereby conferring a mutator phenotype [60]. However, the role of variants in the polymerase active domain of POLD1 remains unknown. In addition to $POLD1^{R689W}$ [60, 61] only one further variant within the polymerase active domain, namely $POLD1^{L604K}$ of mice Polδ, has been described to be potentially pathogenic [95]. Yet, there is growing evidence that base selectivity defects, as induced by $POLD1^{R689W}$, which occur in tumors, might result in dramatic consequences for genome stability [60]. Thus, our data now demonstrated that variants in the polymerase active domain of POLD1, e. g. R689W, can be functionally significant and could confer a similar pathogenic phenotype, as reported variants within the proofreading exonuclease domain.

5.2.6 Future studies

Multiple *POLD1* variants in different cancers have been identified [7, 74, 94], however, their significance remains unknown. Therefore, in this dissertation we characterized several *POLD1* variants, including $POLD1^{R689W}$, by establishing a suitable KO model and applying multiple molecular read-outs. Future studies are mandatory to further validate both the KO model and molecular read-outs as well as the clinical significance of $POLD1^{R689W}$ and other known *POLD1* variants. Mechanistically, we assessed the impact of the $POLD1^{R689W}$ variant on the compensatory activation of the *ATR* pathway and the DNA replication process. Similar to the approach by Hocke *et al.* [41] using *siPOLD1*, the effects of $POLD1^{R689W}$ on the cell cycle progression and apoptosis should be investigated next. In fact, our preliminary data indicate that S-phase arrest and an increased sub-G_1 fraction with concomitant cleavage of PARP and caspase 3 are induced exclusively in $POLD1^{R689W/-}$ cells upon treatment with the ATR inhibitor AZD6738. The fact that, due to the unexpected low tumor take rate, we could only analyze four mice in the clinically relevant group of AZD6738-treated $POLD1^{R689W/-}$ tumors of the *in vivo* experiments, is an important limitation of our study. Therefore, it is necessary to obtain data from additional samples to achieve statistically unambiguous results, which is currently in progress. The KO model we established here together with the applied molecular read-outs represent an approach to determine the impact of certain *POLD1* VUS as a marker of therapeutic response to ATR pathway inhibitors. Thus, the characterization of more *POLD1* variants in different cancer cell lines should be the aim of future stud-

ies. For this purpose, multiple human CRC cell lines would be available, including SNU-C4 and its POLD1^{H863R} variant within the polymerase active domain, HT115 and its POLD1^{R306H} variant as well as LoVo and its POLD1^{V312M} variant, both within the proofreading exonuclease domain. Additionally, by using knock-in models any other variant could be engineered and characterized. From a clinical perspective, it would be interesting to obtain and analyze tumor samples from patients receiving ATR inhibitors in regard to CHK1 phosphorylation, and correlate these data with therapeutic response. Finally, these data could provide the basis for catalogizing *POLD1* variants and their functional impact regarding the sensitization of cancer cells to ATR pathway inhibitors.

5.3 Conclusion

This dissertation was divided into two subprojects, characterizing on the one hand the synthetic lethal relationship between *ATR* and *PRIM1* by demonstrating that *PRIM1* inactivation sensitized cancer cells to ATR and CHK1 inhibitors via S-phase stasis and Wee1-mediated, caspase 8-dependent apoptosis. Variants in *PRIM1* or other components of the Polα-primase complex could thus represent a novel concept for the individualized cancer therapy, as has similarly and previously been proposed for *POLD1* [41]. Vice versa, cancer cells naturally harboring inactivating *ATR* or *CHK1* variants might exhibit increased sensitivity to inhibitors targeting any component of the Polα-primase complex. On the other hand, we demonstrated the significant impact of the POLD1^{R689W} variant on the cellular sensitivity to ATR and CHK1 inhibitors *in vitro* and *in vivo* by establishing a CRISPR/Cas9-mediated *POLD1*-KO model. This model along with the easily applied molecular read-out of CHK1 phosphorylation could thus facilitate an individualized, genotype-based concept to assess the VUS-mediated increased sensitivity of cancers to a therapy with ATR pathway inhibitors. Taken together with the in the literature identified VUS of *POLD1* and *POLE* [7, 74, 94] as well as defects in other polymerases in cancer this dissertation illustrates the emerging role of tumor-specific alterations in DNA polymerases as novel therapeutic targets. The comprehensive identification and functional characterization of all polymerases and their possible synthetic lethal partners is thus essential in future studies.

6 Abstract

The chemical inhibition of the kinase ATR, a central regulator of the DNA damage response, eliminates subsets of cancer cells in different tumors. This effect is at least partly attributable to the synthetic lethal relationship between *ATR* and certain DNA repair genes. In a previous study of our laboratory, *POLD1* and *PRIM1* were identified to act synthetically lethal with *ATR*. Thus, this dissertation was divided into two subprojects to characterize the synthetic lethal relationship between *ATR* and each of the two identified proteins individually.

The first subproject addressed the characterization of the synthetic lethal relationship between *ATR* and *PRIM1*, the catalytic subunit of primase of the polymerase α-primase complex. Applying a genetic *ATR* knock-in model of colorectal cancer cells, we confirmed that siRNA-mediated *PRIM1* depletion inhibits proliferation of *ATR*-deficient cells, and excluded both off-target effects of the applied siRNA targeting *PRIM1*, and artifacts due to clonal variation by using an *ATR* re-expressing cell clone. We expanded these data by demonstrating in a panel of different cancer cell lines that not only genetically induced *ATR* deficiency but also chemical inhibition of ATR or its main effector kinase CHK1 inhibits proliferation upon *PRIM1* depletion. Mechanistically, *PRIM1* depletion in *ATR*-deficient cells caused S-phase stasis with no evidence for increased DNA damage followed by Wee1-mediated activation of caspase 8 and consequently of apoptosis. As *PRIM1* inactivation sensitizes cancer cells to ATR and CHK1 inhibitors, alterations in *PRIM1* or other components of the polymerase α-primase complex could represent a novel concept for the individualized cancer therapy using ATR pathway inhibitors.

The second subproject addressed the further characterization of the synthetic lethal relationship between *ATR* and *POLD1*, the catalytic subunit of polymerase δ.

In the previous study of our laboratory, we demonstrated that not only genetically induced *ATR* deficiency but also chemical inhibition of the ATR pathway inhibits proliferation upon *POLD1* depletion. To extend these data, we now characterized the impact of defined *POLD1* variants on the sensitivity to ATR pathway inhibitors. Therefore, we used the CRISPR/Cas9 technique in the colorectal cancer cell line DLD-1, which harbors four heterozygous *POLD1* variants, to establish heterozygous *POLD1*-knockout clones with exclusive expression of distinct *POLD1* variants. These knockout clones served as a model to determine the functional significance of individual *POLD1* variants. We demonstrated that of the four variants analyzed only POLD1^{R689W} impairs POLD1 function, as shown by compensatory ATR pathway activation and impaired DNA replication. Moreover, the POLD1^{R689W} variant in cancer cells led to a strong decrease of cell survival *in vitro* and decelerated growth of murine xenograft tumors *in vivo* upon treatment with ATR pathway inhibitors, which further corroborates a potential clinical relevance of our data. Our here established and characterized functional model could thus be used to complement algorithm-based models to predict the pathogenicity of tumor-specific variants of uncertain significance, and improve their accuracy. Furthermore, our data enable a novel and potentially clinically relevant concept for the individualized and genotype-based therapy of *POLD1*-deficient cancers with ATR pathway inhibitors.

Taken together with the in the literature identified variants of uncertain significance of *POLD1* and *POLE* as well as defects in other polymerases in cancer the data of this dissertation illustrate the emerging role of tumor-specific alterations in DNA polymerases as novel therapeutic targets. The comprehensive identification and functional characterization of all polymerases and their possible synthetic lethal partners is thus essential in future studies.

7 Zusammenfassung

Die chemische Inhibition der Kinase ATR, einem zentralen Regulator der *DNA damage response*, eliminiert Subpopulationen von Krebszellen in verschiedenen Tumoren. Dieser Effekt ist zumindest teilweise der synthetisch letalen Beziehung zwischen *ATR* und bestimmten DNA-Reparaturgenen zuzuschreiben. Eine frühere Studie unseres Labors identifizierte *POLD1* und *PRIM1* als synthetisch letale Partner von *ATR*. Diese Dissertation wurde daher in zwei Teilprojekte untergliedert, um die synthetisch letalen Beziehungen zwischen beiden Partnern mit *ATR* zu charakterisieren.

Das erste Teilprojekt befasste sich mit der Charakterisierung der synthetisch letalen Beziehung zwischen *ATR* und *PRIM1*, der katalytischen Untereinheit der Primase des Polymerase α/Primase-Komplexes. Durch die Verwendung eines genetischen *ATR-knock-in*-Modells in kolorektalen Karzinomzellen bestätigten wir, dass die siRNA-vermittelte *PRIM1*-Depletion die Proliferation *ATR*-defizienter Zellen inhibiert und schlossen sowohl *off-target*-Effekte der verwendeten siRNA gegen *PRIM1* als auch klonale Artefakte durch die Verwendung eines *ATR*-reexprimierenden Zellklons aus. Zusätzlich konnten wir zeigen, dass in einer Reihe verschiedener Krebszelllinien nicht nur die genetisch induzierte *ATR*-Defizienz, sondern auch die chemische Inhibition von ATR oder dessen Haupteffektorkinase CHK1 die Proliferation nach *PRIM1*-Depletion inhibiert. Mechanistisch verursachte die *PRIM1*-Depletion in *ATR*-defizienten Zellen eine Stagnation während der S-Phase ohne Hinweis auf eine erhöhte DNA-Schädigung, gefolgt von einer Wee1-vermittelten Aktivierung von Caspase 8 mit anschließender Apoptose. Da also die *PRIM1*-Inaktivierung Krebszellen auf ATR- und CHK1-Inhibitoren sensitiviert, könnten Defekte in *PRIM1* oder anderen Komponenten des Polymerase α/Primase-Komplexes ein neuartiges Konzept

für die individualisierte Tumortherapie mittels Inhibitoren des ATR-Signalweges darstellen.

Das zweite Teilprojekt befasste sich mit der tiefer gehenden Charakterisierung der synthetisch letalen Beziehung zwischen *ATR* und *POLD1*, der katalytischen Untereinheit der Polymerase δ. So konnte bereits die vorangegangene Studie aus unserem Labor zeigen, dass sowohl die genetisch induzierte *ATR*-Defizienz als auch die chemische Inhibition des ATR-Signalweges die Proliferation nach *POLD1*-Depletion inhibiert. Um diese Daten zu erweitern, charakterisierten wir nun den Einfluss von bestimmten *POLD1*-Varianten auf die Sensitivität gegenüber ATR-Signalweginhibitoren. Dazu verwendeten wir in der kolorektalen Karzinomzelllinie DLD-1, die vier heterozygote *POLD1*-Varianten enthält, die CRISPR/Cas9-Methode, um heterozygote *POLD1-knockout*-Klone mit ausschließlicher Expression einzelner *POLD1*-Varianten zu etablieren. Diese *knockout*-Klone dienten als Modell, um die funktionelle Bedeutung individueller *POLD1*-Varianten zu bestimmen. Anhand einer kompensatorischen ATR-Signalwegaktivierung und einer beeinträchtigten DNA-Replikation konnten wir zeigen, dass von den vier untersuchten Varianten nur $POLD1^{R689W}$ die POLD1-Funktion schädigte. Weiterhin verursachte die $POLD1^{R689W}$-Variante in Krebszellen eine starke Beeinträchtigung des Zellüberlebens *in vitro* und eine Verlangsamung des Wachstums muriner Xenografttumore *in vivo* nach Behandlung mit verschiedenen Inhibitoren des ATR-Signalweges. Dies untermauert zusätzlich die potentiell klinische Relevanz unserer Daten. Unser hier etabliertes und charakterisiertes funktionelles Modell könnte daher verwendet werden, um algorithmus-basierte Modelle, mit der die Pathogenität tumorspezifischer Varianten unklarer Signifikanz vorhergesagt wird, zu komplementieren und deren Genauigkeit zu verbessern. Weiterhin ermöglichen unsere Daten ein neues und potentiell klinisch relevantes Konzept für die individualisierte und Genotyp-basierte Therapie *POLD1*-defizienter Tumore mit ATR-Signalweginhibitoren.

Zusammen mit den in der Literatur identifizierten Varianten unklarer Signifikanz in *POLD1* und *POLE* sowie den Defekten anderer Polymerasen in Tumoren verdeutlichen die Daten dieser Dissertation die zunehmende Bedeutung tumorspezifischer Veränderungen in DNA-Polymerasen als neue therapeutische Zielstrukturen. Daher ist eine umfassende Identifizierung und funktionelle Charakterisierung aller Polymerasen und ihrer möglichen synthetisch letalen Partner in zukünftigen Studien erforderlich.

8 Bibliography

[1] Abdel-Samad R, Aouad P, Gali-Muhtasib H, Sweidan Z, Hmadi R, *et al.* (**2018**): Mechanism of action of the atypical retinoid ST1926 in colorectal cancer: DNA damage and DNA polymerase α. *American Journal of Cancer Research*, *8*(1), 39–55.

[2] Adzhubei IA, Schmidt S, Peshkin L, Ramensky VE, Gerasimova A, *et al.* (**2010**): A method and server for predicting damaging missense mutations. *Nature Methods*, *7*(4), 248–249.

[3] Ahmed D, Eide PW, Eilertsen IA, Danielsen SA, Eknæs M, *et al.* (**2013**): Epigenetic and genetic features of 24 colon cancer cell lines. *Oncogenesis*, *2*, e71.

[4] Awasthi P, Foiani M, & Kumar A (**2015**): ATM and ATR signaling at a glance. *Journal of Cell Science*, *128*(23), 4255–4262.

[5] Aze A, Zhou JC, Costa A, & Costanzo V (**2013**): DNA replication and homologous recombination factors: acting together to maintain genome stability. *Chromosoma*, *122*(5), 401–413.

[6] Barber LJ, Sandhu S, Chen L, Campbell J, Kozarewa I, *et al.* (**2013**): Secondary mutations in BRCA2 associated with clinical resistance to a PARP inhibitor. *The Journal of Pathology*, *229*(3), 422–429.

[7] Bellido F, Pineda M, Aiza G, Valdés-Mas R, Navarro M, *et al.* (**2016**): POLE and POLD1 mutations in 529 kindred with familial colorectal cancer and/or polyposis: review of reported cases and recommendations for genetic testing and surveillance. *Genetics in Medicine*, *18*(4), 325–332.

[8] Belousova EA & Lavrik OI (**2015**): DNA polymerases β and λ and their roles in cell. *DNA Repair*, *29*, 112–126.

[9] Borel F, Lacroix FB, & Margolis RL (**2002**): Prolonged arrest of mammalian cells at the G1/S boundary results in permanent S phase stasis. *Journal of Cell Science*, *115*(Pt 14), 2829–2838.

[10] Bridges CB (**1922**): The Origin of Variations in Sexual and Sex-Limited Characters. *The American Naturalist*, *56*(642), 51–63.

[11] Bryant HE, Schultz N, Thomas HD, Parker KM, Flower D, *et al.* (**2005**): Specific killing of BRCA2-deficient tumours with inhibitors of poly(ADP-ribose) polymerase. *Nature*, *434*(7035), 913–917.

[12] Burgers PMJ & Kunkel TA (**2017**): Eukaryotic DNA Replication Fork. *Annual Review of Biochemistry*, *86*, 417–438.

[13] Chen M & Wang J (**2002**): Initiator caspases in apoptosis signaling pathways. *Apoptosis*, *7*(4), 313–319.

[14] Choi Y, Sims GE, Murphy S, Miller JR, & Chan AP (**2012**): Predicting the functional effect of amino acid substitutions and indels. *PLoS ONE*, *7*(10), e46688.

[15] Claudiani S & Apperley JF (**2018**): The argument for using imatinib in CML. *Hematology*, *2018*(1), 161–167.

[16] Computational Biology Center (Memorial Sloan Kettering Cancer Center) (**2018**): MutationAssessor. Retrieved from http://mutationassessor.org/r3/. Accessed November 27, 2018.

[17] Cortez D, Guntuku S, Qin J, & Elledge SJ (**2001**): ATR and ATRIP: partners in checkpoint signaling. *Science*, *294*(5547), 1713–1716.

[18] Daee DL, Mertz TM, & Shcherbakova PV (**2010**): A cancer-associated DNA polymerase delta variant modeled in yeast causes a catastrophic increase in genomic instability. *Proceedings of the National Academy of Sciences of the United States of America*, *107*(1), 157–162.

[19] Daud AI, Ashworth MT, Strosberg J, Goldman JW, Mendelson D, *et al.* (**2015**): Phase I dose-escalation trial of checkpoint kinase 1 inhibitor MK-8776 as monotherapy and in combination with gemcitabine in patients with advanced solid tumors. *Journal of Clinical Oncology*, *33*(9), 1060–1066.

[20] Division of Genetics (Brigham & Women's Hospital) (**2018**): PolyPhen-2. Retrieved from http://genetics.bwh.harvard.edu/pph2/. Accessed November 27, 2018.

[21] Do K, Doroshow JH, & Kummar S (**2013**): Wee1 kinase as a target for cancer therapy. *Cell Cycle*, *12*(19), 3159–3164.

[22] Dobzhansky T (**1946**): Genetics of natural populations; recombination and variability in populations of Drosophila pseudoobscura. *Genetics*, *31*, 269–290.

[23] Dresler SL, Gowans BJ, Robinson-Hill RM, & Hunting DJ (**1988**): Involvement of DNA polymerase delta in DNA repair synthesis in human fibroblasts at late times after ultraviolet irradiation. *Biochemistry*, *27*(17), 6379–6383.

[24] Druker BJ (**2008**): Translation of the Philadelphia chromosome into therapy for CML. *Blood*, *112*(13), 4808–4817.

[25] Edwards SL, Brough R, Lord CJ, Natrajan R, Vatcheva R, *et al.* (**2008**): Resistance to therapy caused by intragenic deletion in BRCA2. *Nature*, *451*(7182), 1111–1115.

[26] Elsässer HP, Lehr U, Agricola B, & Kern HF (**1992**): Establishment and characterisation of two cell lines with different grade of differentiation derived from one primary human pancreatic adenocarcinoma. *Virchows Archiv B*, *61*(5), 295–306.

[27] Farmer H, McCabe N, Lord CJ, Tutt ANJ, Johnson DA, *et al.* (**2005**): Targeting the DNA repair defect in BRCA mutant cells as a therapeutic strategy. *Nature*, *434*(7035), 917–921.

[28] Flohr T, Dai JC, Büttner J, Popanda O, Hagmüller E, *et al.* (**1999**): Detection of mutations in the DNA polymerase delta gene of human sporadic colorectal cancers and colon cancer cell lines. *International Journal of Cancer*, *80*(6), 919–929.

[29] Friend SH & Oliff A (**1998**): Emerging uses for genomic information in drug discovery. *The New England Journal of Medicine*, *338*(2), 125–126.

[30] Gallmeier E, Hucl T, Calhoun ES, Cunningham SC, Bunz F, *et al.* (**2007**): Gene-specific selection against experimental fanconi anemia gene inactivation in human cancer. *Cancer Biology & Therapy*, *6*(5), 654–660.

[31] Gallmeier E, Hermann PC, Mueller MT, Machado JG, Ziesch A, *et al.* (**2011**): Inhibition of ataxia telangiectasia- and Rad3-related function

abrogates the in vitro and in vivo tumorigenicity of human colon cancer cells through depletion of the CD133(+) tumor-initiating cell fraction. *Stem Cells*, *29*(3), 418–429.

[32] Ganai RA, Bylund GO, & Johansson E (**2015**): Switching between polymerase and exonuclease sites in DNA polymerase ε. *Nucleic Acids Research*, *43*(2), 932–942.

[33] Garattini E, Parrella E, Diomede L, Gianni M, Kalac Y, *et al.* (**2004**): ST1926, a novel and orally active retinoid-related molecule inducing apoptosis in myeloid leukemia cells: modulation of intracellular calcium homeostasis. *Blood*, *103*(1), 194–207.

[34] Garimella SV, Rocca A, & Lipkowitz S (**2012**): WEE1 inhibition sensitizes basal breast cancer cells to TRAIL-induced apoptosis. *Molecular Cancer Research*, *10*(1), 75–85.

[35] Gesellschaft der epidemiologischen Krebsregister in Deutschland (**2018**): Atlas der Krebsinzidenz und –mortalität in Deutschland (GEKID-Atlas). Datenlieferung: Juli 2017. Retrieved from http://www.gekid.de. Accessed November 15, 2018.

[36] Grabocka E, Pylayeva-Gupta Y, Jones MJK, Lubkov V, Yemanaberhan E, *et al.* (**2014**): Wild-type H- and N-Ras promote mutant K-Ras-driven tumorigenesis by modulating the DNA damage response. *Cancer Cell*, *25*(2), 243–256.

[37] Han T, Goralski M, Capota E, Padrick SB, Kim J, *et al.* (**2016**): The antitumor toxin CD437 is a direct inhibitor of DNA polymerase α. *Nature Chemical Biology*, *12*(7), 511–515.

[38] Hartman JL, Garvik B, & Hartwell L (**2001**): Principles for the buffering of genetic variation. *Science*, *291*(5506), 1001–1004.

[39] Hartwell LH, Szankasi P, Roberts CJ, Murray AW, & Friend SH (**1997**): Integrating genetic approaches into the discovery of anticancer drugs. *Science*, *278*(5340), 1064–1068.

[40] Henninger EE & Pursell ZF (**2014**): DNA polymerase ε and its roles in genome stability. *IUBMB life*, *66*(5), 339–351.

[41] Hocke S, Guo Y, Job A, Orth M, Ziesch A, *et al.* (**2016**): A synthetic lethal screen identifies ATR-inhibition as a novel therapeutic approach for POLD1-deficient cancers. *Oncotarget*, *7*(6), 7080–7095.

[42] Hurley PJ, Wilsker D, & Bunz F (**2007**): Human cancer cells require ATR for cell cycle progression following exposure to ionizing radiation. *Oncogene*, *26*(18), 2535–2542.

[43] J Craig Venter Institute (**2018**): PROVEAN Protein. Retrieved from http://provean.jcvi.org/seq_submit.php. Accessed November 27, 2018.

[44] Jain R, Aggarwal AK, & Rechkoblit O (**2018**): Eukaryotic DNA polymerases. *Current Opinion in Structural Biology*, *53*, 77–87.

[45] Jiang G & Sancar A (**2006**): Recruitment of DNA damage checkpoint proteins to damage in transcribed and nontranscribed sequences. *Molecular and Cellular Biology*, *26*(1), 39–49.

[46] Kaelin WG (**2005**): The concept of synthetic lethality in the context of anticancer therapy. *Nature Reviews Cancer*, *5*(9), 689–698.

[47] Karnitz LM & Zou L (**2015**): Molecular Pathways: Targeting ATR in Cancer Therapy. *Clinical Cancer Research*, *21*(21), 4780–4785.

[48] Ku JL, Yoon KA, Kim DY, & Park JG (**1999**): Mutations in hMSH6 alone are not sufficient to cause the microsatellite instability in colorectal cancer cell lines. *European Journal of Cancer*, *35*(12), 1724–1729.

[49] Kuchta RD, Reid B, & Chang LM (**1990**): DNA primase. Processivity and the primase to polymerase alpha activity switch. *The Journal of Biological Chemistry*, *265*(27), 16158–16165.

[50] Kuriyama I, Asano N, Kato I, Ikeda K, Takemura M, *et al.* (**2005**): Dipeptide alcohol-based inhibitors of eukaryotic DNA polymerase alpha. *Bioorganic & Medicinal Chemistry*, *13*(6), 2187–2196.

[51] Kuriyama I, Fukudome K, Kamisuki S, Kuramochi K, Tsubaki K, *et al.* (**2008**): The specific inhibitory effect of demethoxydehydroaltenusin, a derivative of dehydroaltenusin, on mammalian DNA polymerase alpha. *International Journal of Molecular Medicine*, *22*(6), 793–799.

[52] Lavanya V, Mohamed Adil A, Neesar A, Arun KR, & Shazia J (**2014**): Small molecule inhibitors as emerging cancer therapeutics. *Integrative Cancer Science and Therapeutics*, *1*(3), 39–46.

[53] Lecona E & Fernandez-Capetillo O (**2018**): Targeting ATR in cancer. *Nature Reviews Cancer*, *18*(9), 586–595.

[54] Lee WH, Chen LC, Lee CJ, Huang CC, Ho YS, *et al.* (**2018**): DNA primase polypeptide 1 (PRIM1) involves in estrogen-induced breast cancer formation through activation of the G2/M cell cycle checkpoint. *International Journal of Cancer*.

[55] Lord CJ & Ashworth A (**2017**): PARP inhibitors: Synthetic lethality in the clinic. *Science*, *355*(6330), 1152–1158.

[56] Maeda N, Kamisuki S, Takahashi S, Yoshida H, Sakaguchi K, *et al.* (**2006**): The In Vitro and In Vivo Inhibitory Effect of Dehydroaltenusin: A Specific Inhibitor of Mammalian DNA Polymerase α. *Current Bioactive Compounds*, *2*(1), 3–11.

[57] Masai H, Matsumoto S, You Z, Yoshizawa-Sugata N, & Oda M (**2010**): Eukaryotic chromosome DNA replication: where, when, and how? *Annual Review of Biochemistry*, *79*, 89–130.

[58] Matheson CJ, Backos DS, & Reigan P (**2016**): Targeting WEE1 Kinase in Cancer. *Trends in Pharmacological Sciences*, *37*(10), 872–881.

[59] McCulloch SD, Kokoska RJ, Masutani C, Iwai S, Hanaoka F, *et al.* (**2004**): Preferential cis-syn thymine dimer bypass by DNA polymerase eta occurs with biased fidelity. *Nature*, *428*(6978), 97–100.

[60] Mertz TM, Sharma S, Chabes A, & Shcherbakova PV (**2015**): Colon cancer-associated mutator DNA polymerase δ variant causes expansion of dNTP pools increasing its own infidelity. *Proceedings of the National Academy of Sciences of the United States of America*, *112*(19), E2467–2476.

[61] Mertz TM, Baranovskiy AG, Wang J, Tahirov TH, & Shcherbakova PV (**2017**): Nucleotide selectivity defect and mutator phenotype conferred by a colon cancer-associated DNA polymerase δ mutation in human cells. *Oncogene*, *36*(31), 4427–4433.

[62] Mizushina Y, Kamisuki S, Mizuno T, Takemura M, Asahara H, *et al.* (**2000**): Dehydroaltenusin, a mammalian DNA polymerase alpha inhibitor. *The Journal of Biological Chemistry*, *275*(43), 33957–33961.

[63] Molinari M, Mercurio C, Dominguez J, Goubin F, & Draetta GF (**2000**): Human Cdc25 A inactivation in response to S phase inhibition and its role in preventing premature mitosis. *EMBO Reports*, *1*(1), 71–79.

[64] Muller PAJ & Vousden KH (**2014**): Mutant p53 in cancer: new functions and therapeutic opportunities. *Cancer Cell*, *25*(3), 304–317.

[65] Muñoz-Pinedo C, El Mjiyad N, & Ricci JE (**2012**): Cancer metabolism: current perspectives and future directions. *Cell Death & Disease*, *3*, e248.

[66] Nepal M, Che R, Zhang J, Ma C, & Fei P (**2017**): Fanconi Anemia Signaling and Cancer. *Trends in Cancer*, *3*(12), 840–856.

[67] Nicolas E, Golemis EA, & Arora S (**2016**): POLD1: Central mediator of DNA replication and repair, and implication in cancer and other pathologies. *Gene*, *590*(1), 128–141.

[68] Nicoletti I, Migliorati G, Pagliacci MC, Grignani F, & Riccardi C (**1991**): A rapid and simple method for measuring thymocyte apoptosis by propidium iodide staining and flow cytometry. *Journal of Immunological Methods*, *139*(2), 271–279.

[69] Nieminuszczy J, Schwab RA, & Niedzwiedz W (**2016**): The DNA fibre technique – tracking helicases at work. *Methods*, *108*, 92–98.

[70] Nijman SMB (**2011**): Synthetic lethality: general principles, utility and detection using genetic screens in human cells. *FEBS Letters*, *585*(1), 1–6.

[71] Niroula A, Urolagin S, & Vihinen M (**2015**): PON-P2: prediction method for fast and reliable identification of harmful variants. *PLoS ONE*, *10*(2), e0117380.

[72] Nishida C, Reinhard P, & Linn S (**1988**): DNA repair synthesis in human fibroblasts requires DNA polymerase delta. *The Journal of Biological Chemistry*, *263*(1), 501–510.

[73] O'Driscoll M, Ruiz-Perez VL, Woods CG, Jeggo PA, & Goodship JA (**2003**): A splicing mutation affecting expression of ataxia-telangiectasia and Rad3-related protein (ATR) results in Seckel syndrome. *Nature Genetics*, *33*(4), 497–501.

[74] Palles C, Cazier JB, Howarth KM, Domingo E, Jones AM, *et al.* (**2013**): Germline mutations affecting the proofreading domains of POLE and POLD1 predispose to colorectal adenomas and carcinomas. *Nature Genetics*, *45*(2), 136–144.

[75] Parplys AC, Petermann E, Petersen C, Dikomey E, & Borgmann K (**2012**): DNA damage by X-rays and their impact on replication processes. *Radiotherapy and Oncology*, *102*(3), 466–471.

[76] Patil M, Pabla N, & Dong Z (**2013**): Checkpoint kinase 1 in DNA damage response and cell cycle regulation. *Cellular and Molecular Life Sciences*, *70*(21), 4009–4021.

[77] Pellegrini L (**2012**): The Pol α-primase complex. *Subcellular Biochemistry*, *62*, 157–169.

[78] Pihlak R, Valle JW, & McNamara MG (**2017**): Germline mutations in pancreatic cancer and potential new therapeutic options. *Oncotarget*, *8*(42), 73240–73257.

[79] Protein Structure and Bioinformatics Group (Lund University) (**2018**): PON-P2. Retrieved from http://structure.bmc.lu.se/PON-P2/. Accessed November 27, 2018.

[80] Reaper PM, Griffiths MR, Long JM, Charrier JD, Maccormick S, *et al.* (**2011**): Selective killing of ATM- or p53-deficient cancer cells through inhibition of ATR. *Nature Chemical Biology*, *7*(7), 428–430.

[81] Reva B, Antipin Y, & Sander C (**2011**): Predicting the functional impact of protein mutations: application to cancer genomics. *Nucleic Acids Research*, *39*(17), e118.

[82] Richards S, Aziz N, Bale S, Bick D, Das S, *et al.* (**2015**): Standards and guidelines for the interpretation of sequence variants: a joint consensus recommendation of the American College of Medical Genetics and Genomics and the Association for Molecular Pathology. *Genetics in Medicine*, *17*(5), 405–424.

[83] Rogakou EP, Pilch DR, Orr AH, Ivanova VS, & Bonner WM (**1998**): DNA double-stranded breaks induce histone H2AX phosphorylation on serine 139. *The Journal of Biological Chemistry*, *273*(10), 5858–5868.

[84] Rundle S, Bradbury A, Drew Y, & Curtin NJ (**2017**): Targeting the ATR-CHK1 Axis in Cancer Therapy. *Cancers*, *9*(5).

[85] Russell PJ, iGenetics: A Molecular Approach (Benjamin Cummings, San Francisco, **2010**), 3rd edition.

[86] Ruzankina Y, Schoppy DW, Asare A, Clark CE, Vonderheide RH, *et al.* (**2009**): Tissue regenerative delays and synthetic lethality in adult mice after combined deletion of Atr and Trp53. *Nature Genetics*, *41*(10), 1144–1149.

[87] Sanger Institute (**2018**): Catalogue Of Somatic Mutations In Cancer (COSMIC). Retrieved from http://cancer.sanger.ac.uk/cosmic. Accessed November 22, 2018.

[88] Sangster-Guity N, Conrad BH, Papadopoulos N, & Bunz F (**2011**): ATR mediates cisplatin resistance in a p53 genotype-specific manner. *Oncogene*, *30*(22), 2526–2533.

[89] Scagliotti G, Kang JH, Smith D, Rosenberg R, Park K, *et al.* (**2016**): Phase II evaluation of LY2603618, a first-generation CHK1 inhibitor, in combination with pemetrexed in patients with advanced or metastatic non-small cell lung cancer. *Investigational New Drugs*, *34*(5), 625–635.

[90] Statistisches Bundesamt (Destatis) (**2019**): Todesursachen in Deutschland - Fachserie 12 Reihe 4 - 2015. Retrieved from https://www.destatis.de/DE/Publikationen/Thematisch/Gesundheit/Todesursachen/Todesursachen.html. Accessed January 07, 2019.

[91] Tominaga Y, Li C, Wang RH, & Deng CX (**2006**): Murine Wee1 plays a critical role in cell cycle regulation and pre-implantation stages of embryonic development. *International Journal of Biological Sciences*, *2*(4), 161–170.

[92] Uchimura A, Hidaka Y, Hirabayashi T, Hirabayashi M, & Yagi T (**2009**): DNA polymerase delta is required for early mammalian embryogenesis. *PLoS ONE*, *4*(1), e4184.

[93] Vaisman A & Woodgate R (**2017**): Translesion DNA polymerases in eukaryotes: what makes them tick? *Critical Reviews in Biochemistry and Molecular Biology*, *52*(3), 274–303.

[94] Valle L, Hernández-Illán E, Bellido F, Aiza G, Castillejo A, *et al.* (**2014**): New insights into POLE and POLD1 germline mutations in familial colorectal cancer and polyposis. *Human Molecular Genetics*, *23*(13), 3506–3512.

[95] Venkatesan RN, Treuting PM, Fuller ED, Goldsby RE, Norwood TH, *et al.* (**2007**): Mutation at the polymerase active site of mouse DNA polymerase delta increases genomic instability and accelerates tumorigenesis. *Molecular and Cellular Biology*, *27*(21), 7669–7682.

[96] Viallard C & Larrivée B (**2017**): Tumor angiogenesis and vascular normalization: alternative therapeutic targets. *Angiogenesis*, *20*(4), 409–426.

[97] Waga S & Stillman B (**1998**): The DNA replication fork in eukaryotic cells. *Annual Review of Biochemistry*, *67*, 721–751.

[98] Wagner JM & Kaufmann SH (**2010**): Prospects for the Use of ATR Inhibitors to Treat Cancer. *Pharmaceuticals*, *3*(5), 1311–1334.

[99] Webster JA, Tibes R, Morris L, Blackford AL, Litzow M, *et al.* (**2017**): Randomized phase II trial of cytosine arabinoside with and without the CHK1 inhibitor MK-8776 in relapsed and refractory acute myeloid leukemia. *Leukemia Research*, *61*, 108–116.

[100] Welsh JL, Hoskin TL, Day CN, Thomas AS, Cogswell JA, *et al.* (**2017**): Clinical Decision-Making in Patients with Variant of Uncertain Significance in BRCA1 or BRCA2 Genes. *Annals of Surgical Oncology*, *24*(10), 3067–3072.

[101] Wilsker D & Bunz F (**2007**): Loss of ataxia telangiectasia mutated- and Rad3-related function potentiates the effects of chemotherapeutic drugs on cancer cell survival. *Molecular Cancer Therapeutics*, *6*(4), 1406–1413.

[102] Xu H, Ma J, Wu J, Chen L, Sun F, *et al.* (**2016**): Gene expression profiling analysis of lung adenocarcinoma. *Brazilian Journal of Medical and Biological Research*, *49*(3), e4861.

[103] Yarbro JW (**1992**): Mechanism of action of hydroxyurea. *Seminars in Oncology*, *19*(3 Suppl 9), 1–10.

[104] Yotov WV, Hamel H, Rivard GE, Champagne MA, Russo PA, *et al.* (**1999**): Amplifications of DNA primase 1 (PRIM1) in human osteosarcoma. *Genes, Chromosomes & Cancer*, *26*(1), 62–69.

A
Appendix

Figure 17 | Map of the Cas9 plasmid
Schematic depiction of the Cas9 plasmid used for the KO of *POLD1* in DLD-1 cells via CRISPR/Cas9.

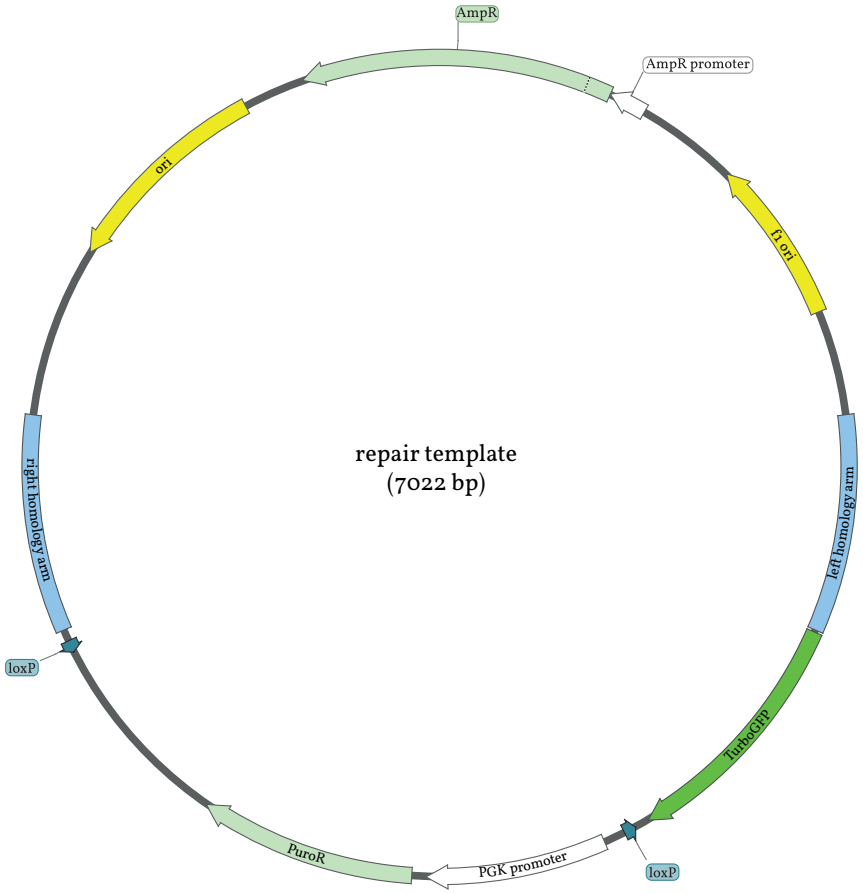

Figure 18 | Map of the repair template plasmid
Schematic depiction of the repair template plasmid used for the KO of *POLD1* in DLD-1 cells via CRISPR/Cas9.

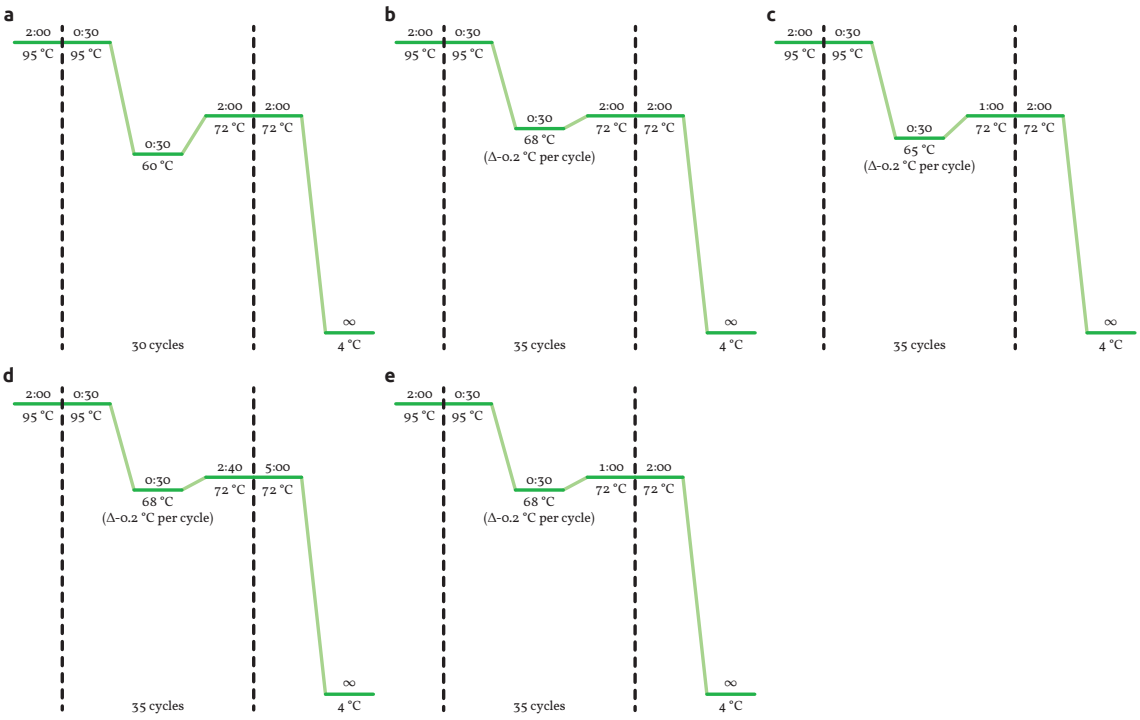

Figure 19 | PCR programs
a–e | All PCR programs used in this dissertation for the amplification of DNA fragments.

Table 10 | PCR conditions

Primer[a]	PCR program[b]	Aim	PCR product
#1 – #4	(a)	genotyping of the *POLD1*-KO status after CRISPR/Cas9 application	1656 bp (WT allele) 1000 bp (KO allele)
#5 + #6	(b)	genotyping of the PuroR cassette after Cre transfection	1759 bp (Cre/loxP +) / (Cre/loxP -)
#7 – #12	(c)	genomic DNA amplification for sequencing exons 13, 17, and 18 (using primers #S2 – #S4)	440 bp (exon 13) 478 bp (exon 17) 266 bp (exon 18)
#1 + #4	(a)	genomic DNA amplification for sequencing *POLD1* exon 2a (using primer #S1)	1656 bp
#13 + #14	(d)	mRNA amplification of *POLD1* exons 2a–21, serving as template for a nested PCR[c]	2581 bp
#15 + #16	(e)	amplification of the nested PCR amplicon for sequencing *POLD1* exon 13 (using primer #S5)	627 bp
#17 + #18	(e)	amplification of the nested PCR amplicon for sequencing *POLD1* exon 17 and 18 (using primer #S6)	697 bp

[a] according to Table 8

[b] according to Figure 19

[c] nested PCR amplicon 1:200 diluted for subsequent PCR reactions

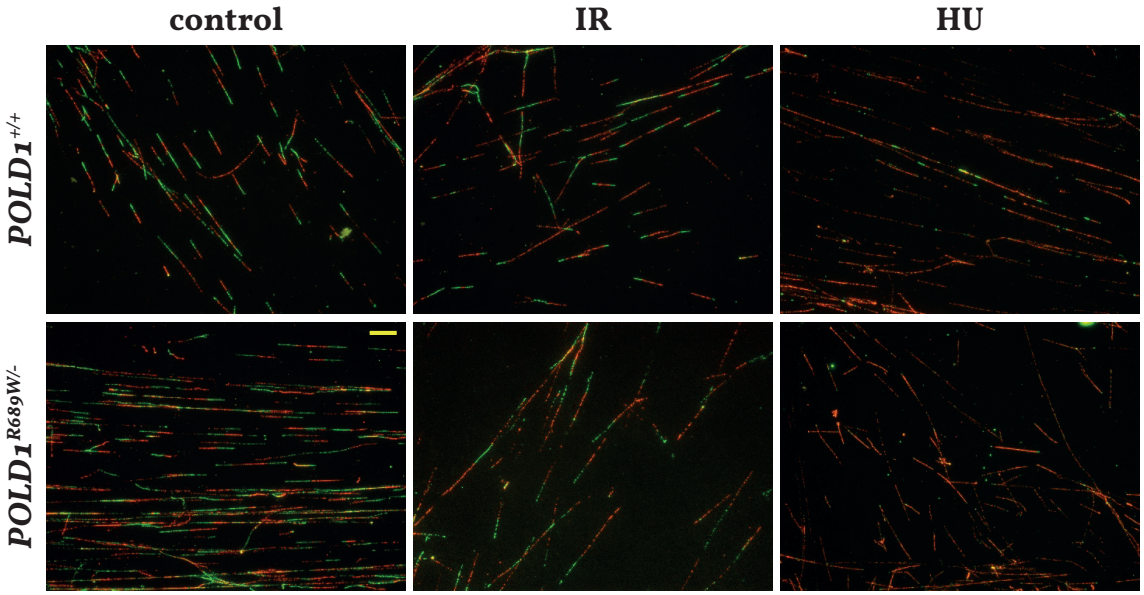

Figure 20 | Representative depiction of DNA fibers
Representative depiction of DNA fibers of *POLD1*$^{+/+}$ and *POLD1*$^{R689W/-}$ cells without treatment as well as upon IR or HU treatment to quantify ongoing replication (red-green), stalled forks (red), and 2nd pulse origins (green). Scale bar equals 10 µm.

A.1 Publications

Original articles:

Job A, Tatura M, Schäfer C, Zielinski A, Borgmann K, Gress TM, Buchholz M & Gallmeier E: Mutations of *POLD1* increase the sensitivity of colorectal cancer cells to ATR and CHK1 inhibitors. *Manuscript in preparation.*

Job A, Schmitt LM, von Wenserski L, Lankat-Buttgereit B, Gress TM, Buchholz M & Gallmeier E (2018): Inactivation of PRIM1 Function Sensitizes Cancer Cells to ATR and CHK1 Inhibitors. *Neoplasia, 20*(11), 1135–1143.
DOI: 10.1016/j.neo.2018.08.009

Hocke S, Guo Y, **Job A**, Orth M, Ziesch A, Lauber K, De Toni EN, Gress TM, Herbst A, Göke B & Gallmeier E (2016): A synthetic lethal screen identifies ATR-inhibition as a novel therapeutic approach for POLD1-deficient cancers. *Oncotarget, 7*(6), 7080–7095.
DOI: 10.18632/oncotarget.6857

Brösicke N, Sallouh M, Prior LM, **Job A**, Weberskirch R & Faissner A (2015): Extracellular Matrix Glycoprotein-Derived Synthetic Peptides Differentially Modulate Glioma and Sarcoma Cell Migration. *Cellular and Molecular Neurobiology, 35*(5): 741–753.
DOI: 10.1007/s10571-015-0170-1

Abstracts and congress contributions:

Job A, Schmitt LM, von Wenserski L, Lankat-Buttgereit B, Gress TM, Buchholz M & Gallmeier E (2018): *PRIM1* als Zielstruktur für neue Therapieansätze in gastrointestinalen Tumoren. *Zeitschrift für Gastroenterologie, 56*(08), e297.
DOI: 10.1055/s-0038-1668908

Job A, Tatura M, Schäfer C, Gress TM, Buchholz M & Gallmeier E (2018): *POLD1*-Mutationen sensitivieren kolorektale Tumorzellen auf ATR-Inhibitoren im Mausmodell. *Zeitschrift für Gastroenterologie, 56*(08), e296.
DOI: 10.1055/s-0038-1668904

Job A, Schäfer C, Buchholz M, GressTM & Gallmeier E (2017): *POLD1*-Mutationen als prädiktiver Marker für das Ansprechen auf ATR-Inhibitoren in gastrointestinalen Tumoren. *Zeitschrift für Gastroenterologie, 55*(08), e57-e299.
DOI: 10.1055/s-0037-1604871

A.2 Curriculum vitae

A.3 Academic teachers

The following gentlemen were my academic teachers at the Philipps-Universität Marburg:

Buchholz, Malte
Gallmeier, Eike

The following ladies and gentlemen were my academic teachers at the Ruhr-Universität Bochum:

Faissner, Andreas
Herlitze, Stefan
Jaquet, Kornelia
Mosig, Axel
Tenbusch, Matthias
Überla, Klaus
Wiese, Stefan

The following ladies and gentlemen were my academic teachers at the Rheinische Friedrich-Wilhelms-Universität Bonn:

Ahmadi, Seifollah
Baader, Stephan
Bajorath, Jürgen
Bauer, Reinhard
Baur, Max P.
Bieber, Thomas
Bierbaum, Gabriele
Bönisch, Heinz
Brinkmann, Kai-Thomas
Bruchhausen, Walter
Brüstle, Oliver
Cichon, Sven Jörg
Degen, Joachim
Drosten, Christian
Eckhardt, Matthias
Edenhofer, Frank
Eis-Hübinger, Anna Maria
Engel, Daniel Robert
Famulok, Michael
Fleischmann, Bernd
Franz, Thomas
Gieselmann, Volkmar
Haas, Albert
Hartmann, Dieter
Hartmann, Gunther
Hartmann, Wolfgang
Hesse, Michael
Hoch, Michael
Höhfeld, Jörg
Hörauf, Achim
Huang, Ruijing
Jäger, Richard
Jahn, Rainer
Janzen, Viktor
Kalff, Jörg
Kappler, Joachim
Kirfel, Jutta
Knolle, Percy
Koch, Norbert
Kolanus, Waldemar
von Kügelgen, Ivar
Kümmerer, Beate
Kunz, Wolfram
Kurts, Christian
Lang, Thorsten
Limmer, Andreas
Mader, Werner
Magin, Thomas

Maier, Karl
Matz, Bertfried
Merkelbach-Bruse, Sabine
Mertler, Gunnar
Meyer, Rainer
Miething, Andreas
Montag, Markus
Müller, Marcel
Neumann, Harald
Nöthen, Markus
Pankratz, Michael
Pfarr, Kenneth
Piel, Joern
Sahl, Hans-Georg
Scheffler, Björn
Schildgen, Oliver Ernst
Schildhaus, Hans-Ulrich
Schilling, Karl
Schmandt-Kappel, Tanja
Schorle, Hubert
Schultze, Joachim
Schumacher, Johannes
Specht, Sabine
Spengler, Ulrich
Swandulla, Dieter
Thoma, Ulrike
Tüting, Thomas
Voos, Wolfgang
Walter, Jochen
Wardelmann, Eva
Weber, Ruthild Gisela
Wenzel, Jörg Albert
Wernig, Anton
Wiedemann, Imke

A.4 Acknowledgment

Foremost, I like to express my sincere gratitude to my doctoral advisor Eike Gallmeier for his excellent supervision during the last couple of years. Whenever it was necessary, he took the time to discuss data, problems, or potential new projects, and never lost his patience, a fact that I did not take for granted considering the plenty of his clinical responsibilities. I enjoyed working in his lab group, and, most importantly, I learned a lot during my PhD studies.

Special thanks also go to Malte Buchholz for his always open door and the time he took to answer my many questions.

I like to thank Thomas M. Gress for providing the laboratory facilities and the financial support of my work.

I am grateful to the former and present members of the lab group of Eike Gallmeier—Bettina Geisel, Brigitte Lankat-Buttgereit, Lisa von Wenserski, Lisa-Maria Schmitt, and Cora Schäfer—and of course to the members of the lab group of Malte Buchholz—especially Marina Tatura and Lisa Eick—for their support, their help, the important scientific coffee breaks, and the great working atmosphere, which made it so much easier to complete my PhD studies.

Last but most certainly not least I owe my family the deepest gratitude for their constant and unconditional support, help, motivation, and encouragement. Everything that I accomplished is due to my family and therefore I will always be thankful.

A.5 Ehrenwörtliche Erklärung